Trans-Modulation of the Somatostatin Type 2A Receptor Trafficking by Insulin-Regulated Aminopeptidase Decreases Limbic Seizures

D. de Bundel, A. Fafouri, Z. Csaba, E. Loyens, S. Lebon, V. El Ghouzzi, S. Peineau, G. Vodjdani, F. Kiagiadaki, N. Aourz, et al.

The Journal of Neuroscience

http://jneurosci.msubmit.net

JN-RM-0476-15R1

Trans-modulation of the somatostatin type 2A receptor trafficking by Insulin-regulated aminopeptidase decreases limbic seizures

Pascal Dournaud, Inserm U1141
Dimitri De Bundel, Center for Neurosciences, Vrije Universiteit Brussel
Assia Fafouri, Inserm U1141
Zsolt Csaba, zsolt.csaba@inserm.fr
Ellen Loyens, Center for Neurosciences, Vrije Universiteit
Sophie Lebon, Inserm U1141
Vincent El Ghouzzi, Inserm U1141
Stephane Peineau, Inserm U676
Guilan Vodjdani, PROTECT
Foteini Kiagiadaki, Faculty of Medicine, University of Crete
Najat Aourz, Vrije Universiteit Brussel
Jessica Coppens, Vrije Universiteit Brussel
Laura Walrave, Center for Neurosciences, Vrije Universiteit
Jeanelle Portelli, vrije universiteit brussel
Patrick Vanderheyden, Center for Neurosciences, Vrije Universiteit
Siew Yeen Chai, Department of Physiology, Monash University
Kyriaki Thermos, Faculty of Medicine, University of Crete
Véronique Bernard, CNRS & Université P. & et M. Curie
Graham Collingridge, MRC Centre for Synaptic Plasticity
Stéphane Auvin, Inserm U1141
Pierre Gressens, Hôpital Robert Debré, Inserm
Ilse Smolders, Vrije Universiteit Brussel

Commercial Interest: No

Trans-modulation of the somatostatin type 2A receptor trafficking by Insulin-regulated aminopeptidase decreases limbic seizures

Running title: IRAP regulates sst2A receptor traffic and seizures

Dimitri De Bundel[1]*, Assia Fafouri[2,3]*, Zsolt Csaba[2,3]*, Ellen Loyens[1], Sophie Lebon[2,3], Vincent El Ghouzzi[2,3], Stéphane Peineau[2,3,4], Guilan Vodjdani[2,3], Foteini Kiagiadaki[5], Najat Aourz[1], Jessica Coppens[1], Laura Walrave[1], Jeanelle Portelli[1], Patrick Vanderheyden[6], Siew Yeen Chai[7], Kyriaki Thermos[5], Véronique Bernard[8], Graham Collingridge[4], Stéphane Auvin[2,3], Pierre Gressens[2,3], Ilse Smolders[1]** and Pascal Dournaud[2,3]**

[1] Department of Pharmaceutical Chemistry and Drug Analysis, Center for Neurosciences, Vrije Universiteit Brussel, 1090 Brussels, Belgium
[2] Inserm, U1141, 75019 Paris, France
[3] University Paris Diderot, Sorbonne Paris Cité, UMR1141, 75019 Paris, France
[4] MRC Centre for Synaptic Plasticity; School of Physiology and Pharmacology; University of Bristol; Bristol, UK
[5]Laboratory of Pharmacology, Faculty of Medicine, University of Crete, Heraklion, Greece
[6]Department of Molecular and Biochemical Pharmacology, Vrije Universiteit Brussel, Brussels, Belgium
[7]Department of Physiology, Monash University, Victoria, Australia
[8]Inserm U952, CNRS UMR7224, Université Pierre et Marie Curie, Paris, France

* These authors contributed equally to this work.
** These authors jointly supervised this work.

Corresponding author:
Pascal Dournaud, PhD
pascal.dournaud@inserm.fr
Inserm U1141, Hôpital Robert Debré, 48 Boulevard Sérurier, 75019 Paris, France

Number of pages :		45
Number of figures :		15
Number of words :	Abstract :	213
	Introduction :	500
	Discussion :	1500

Abstract

Within the hippocampus, the major somatostatin (SRIF) receptor subtype, the sst2A receptor, is localized at post-synaptic sites of the principal neurons where it modulates neuronal activity. Following agonist exposure, this receptor rapidly internalizes and recycles slowly through the *trans*-Golgi network. In epilepsy, a high and chronic release of somatostatin occurs which provokes, in both rat and human tissue, a decrease in the density of this inhibitory receptor at the cell surface. The insulin-regulated aminopeptidase (IRAP) is involved in vesicular trafficking and shares common regional distribution with the sst2A receptor. In addition, IRAP ligands display anticonvulsive properties. We therefore sought to assess by *in vitro* and *in vivo* experiments in hippocampal rat tissue whether IRAP ligands could regulate the trafficking of the sst2A receptor and, consequently, modulate limbic seizures. Using pharmacological and cell biological approaches, we demonstrate that IRAP ligands accelerate the recycling of the sst2A receptor that has internalized in neurons *in vitro* or *in vivo*. Most importantly, because IRAP ligands increase the density of this inhibitory receptor at the plasma membrane, they also potentiate the neuropeptide SRIF inhibitory effects on seizure activity. Our results further demonstrate that IRAP is a therapeutic target for the treatment of limbic seizures and possibly for other neurological conditions in which down-regulation of G protein-coupled receptors occurs.

Significance Statement

The somatostatin type 2A receptor (sst2A) is localized on principal hippocampal neurons and displays anticonvulsant properties. Following agonist exposure, however, this receptor rapidly internalizes and recycles slowly. The insulin-regulated aminopeptidase (IRAP) is involved in vesicular trafficking and shares common regional distribution with the sst2A receptor. We therefore assessed by *in vitro* and *in vivo* experiments whether IRAP could regulate the trafficking of this receptor. We demonstrate that IRAP ligands accelerate sst2A recycling in hippocampal neurons. Because IRAP ligands increase the density of sst2A receptors at the plasma membrane, they also potentiate the effects of this inhibitory receptor on seizure activity. Our results further demonstrate that IRAP is a therapeutic target for the treatment of limbic seizures.

Introduction

The somatostatin (SRIF) type 2A receptor (sst2A) mediates SRIF inhibitory effects on cell excitability (Peineau et al., 2003; Olias et al., 2004; Bassant et al., 2005) and displays anticonvulsant properties (Vezzani and Hoyer, 1999; Tallent and Qiu, 2008; Clynen et al., 2014; Dobolyi et al., 2014). Like many GPCRs, sst2A receptors rapidly internalize (Dournaud et al., 1998; Csaba et al., 2001; Csaba et al., 2003; Stumm et al., 2004; Csaba et al., 2012) and are then specifically targeted to a perinuclear/*trans*-Golgi network (TGN) compartment, bypassing the late endosomal compartment and the degradative pathway (Csaba et al., 2007; Lelouvier et al., 2008). Afterwards they slowly recycle to the plasma membrane of both cell bodies and dendrites. Interestingly, this particular recycling route undertaken by the sst2A receptor shares common pathways with the glucose transporter 4 (GLUT4) (Leto and Saltiel, 2012). A key regulator of GLUT4 storage vesicles is the insulin-regulated aminopeptidase (IRAP), a type II membrane protein (Chai et al., 2004; Albiston et al., 2007; Vanderheyden, 2009; Wright and Harding, 2011). In the basal state, IRAP is located principally in an intracellular compartment with GLUT4, and these proteins move to the cell surface identically in response to insulin (Keller, 2003). In addition to its aminopeptidase activity involved in peptide hormone processing, IRAP also acts as a receptor for the endogenous ligands angiotensin IV (Ang IV) and LVV-Hemorphin 7 (LVV-H7). IRAP ligands are on the one hand competitive inhibitors of the enzymatic activity of IRAP and on the other hand regulators of its trafficking (Albiston et al., 2007). The extracellular part of IRAP contains the aminopeptidase activity while its intracellular domain interacts with cytosolic proteins that contribute to GLUT4 vesicles retention and translocation to the plasma membrane, however the mechanisms involved in this latter process remain to be demonstrated (Albiston et al., 2007).

Although the memory- and cognitive-enhancing effects of IRAP ligands are well established (Albiston et al., 2003; Albiston et al., 2011), the role of IRAP in the central nervous

system is yet to be fully elucidated. Most interestingly, IRAP ligands display anticonvulsive activities in different animal models (Tchekalarova et al., 2001; Tchekalarova et al., 2004; Stragier et al., 2006; Loyens et al., 2011). In accordance with these central actions, IRAP was found to be highly expressed in brain areas associated with cognition and epilepsy (Fernando et al., 2005), regions that also displayed the highest densities of sst2A receptor immunoreactivity (Dournaud et al., 1996; Schindler et al., 1997; Dournaud et al., 1998). At the cellular level, IRAP immunoreactivity in neurons is associated with the *trans*-Golgi apparatus and vesicular structures in the proximity of the Golgi cisternae (Fernando et al., 2007), a location remarkably comparable to that of internalized sst2A receptors before recycling (Csaba et al., 2007; Lelouvier et al., 2008). Because IRAP shares common distribution with the sst2A receptor and is involved in vesicular trafficking, we sought to assess by *in vitro* and *in vivo* experiments whether IRAP could regulate the trafficking of the sst2A receptor and, consequently, modulate its anticonvulsant actions.

Material and Methods

Animals. Experimental procedures were performed using adult male Wistar rats (Charles River Laboratories). All efforts were made to reduce the number of animals used and any distress caused by the procedures is in accordance with the European Communities Council Directive of September 22, 2010 (2010/63/UE) and complying with the guidelines of Inserm, the ethics committees on animal experiments of Paris Diderot University, the Vrije Universiteit Brussel and the University of Crete. Accordingly, the number of animals in our study was kept to the necessary minimum.

Antibodies. The endogenous sst2A receptor was immunolocalized using a rabbit monoclonal antibody (3582-1, Epitomics; 1:1000). This antibody is directed towards residues 355–369 of the human sst2A receptor. This sequence is identical in mouse, rat, and human sst2A. Endogenous IRAP was detected using a mouse monoclonal antibody (9876-3E1, Cell Signaling; 1:200) directed against a fusion protein corresponding to the amino terminus of rat IRAP. A sheep polyclonal antibody was used to detect the *trans*-Golgi network (TGN) specific integral membrane protein (TGN38) (PA1-84496, Thermo Scientific; 1:800). Secondary antibodies used were Alexa Fluor 488 (A488)-conjugated donkey anti-rabbit (1:500; Life Technologies, Molecular Probes) or Cyanine 3 (Cy3)-conjugated donkey anti rabbit (1:500; Jackson ImmunoResearch), Cy3-conjugated donkey anti-mouse (1:500; Jackson ImmunoResearch) or A488-conjugated donkey anti-mouse (1:500; Life Technologies, Molecular Probes), and Alexa Fluor 633 (A633)-conjugated donkey anti-sheep (1:500; Life Technologies, Molecular Probes) to immunolocalize sst2A receptor, IRAP and TGN38, respectively. For chromogenic detection of sst2A receptor and IRAP, biotinylated goat anti-rabbit and anti-mouse antibodies (1:300, Vector Laboratories) were used, respectively.

Stereotaxic injection of octreotide. Rats under isoflurane anesthesia were mounted on a stereotaxic frame and injected into the dorsal hippocampus (coordinates: 2.8 mm posterior; 1.4 mm lateral; 3.2 mm ventral from Bregma) with octreotide (OCT; gift from Novartis Pharma AG) as previously described (Csaba et al., 2007). After 3h of survival, rats were deeply anesthetized with sodium pentobarbital (60 mg/kg i.p.) and perfused through the ascending aorta with 400 ml of 4% paraformaldehyde in 0.1 M phosphate buffer, pH 7.4 (PB). Brains were cryoprotected, frozen in liquid isopentane at -45°C and sectioned in the coronal plane at a thickness of 30 μm as previously described (Csaba et al., 2007).

Immunohistochemistry. Brain sections at the level of the dorsal hippocampus were selected for chromogenic and immunofluorescent labeling. For chromogenic labeling, endogenous peroxidase activity was first quenched by 0.3% H_2O_2 in 0.01 M phosphate-buffered saline, pH 7.4 (PBS) for 30 min at room temperature (RT), washed in PBS, incubated in PBS with 5% normal goat serum (NGS; Sigma-Aldrich) and 0.3% Triton X-100 for 30 min at RT, incubated with primary antibodies diluted in PBS with 1% NGS and 0.3% Triton X-100 overnight at RT, rinsed in PBS, incubated in biotinylated secondary antibodies diluted in PBS with 3% NGS and 0.3% Triton X-100 for 1 h at RT, washed in PBS, and incubated in avidin-biotinylated horseradish peroxidase complex (ABC; Vector Laboratories) diluted in PBS for 90 min at RT. Peroxidase activity was revealed with 0.05% of 3,3'-diaminobenzidine (DAB; Sigma-Aldrich) in 0.05 M Tris buffer, pH 7.6 (TB), in the presence of hydrogen peroxide (0.0048%). The reaction was stopped by several washes in TB. Sections were mounted on gelatin-coated slides, dehydrated in graded ethanols, delipidated in xylene and coverslipped with Permount (Fisher Scientific) for light microscopic observation. For immunofluorescent labeling, sections were preincubated in PBS with 5% normal donkey serum (NDS, Sigma-Aldrich) and 0.3% Triton X-100 for 30 min at RT, incubated in primary antibodies diluted in PBS with 1% NDS and 0.3%

Triton X-100 overnight at RT, rinsed in PBS, and incubated in fluorescent secondary antibodies diluted in PBS with 3% NDS and 0.3% Triton X-100 for 1 h at RT. Finally, sections were rinsed in PBS, mounted on glass slides and coverslipped with Fluoromount (Southern Biotech) for confocal microscopic analysis.

Hippocampal cell cultures. Hippocampi were dissected from 18-day-old embryo Wistar rat brains and dissociated in HBSS with 0.25% trypsin and 0.1% DNase 1. Hippocampal neurons were plated on glass coverslips previously coated with gelatin and poly-L-lysine. Neurons were grown in Neurobasal medium (Invitrogen) supplemented with B27 and glutamine (Invitrogen) and maintained in an incubator at 37°C in a 95% air/5% CO_2 humidified atmosphere. All experiments were carried out at 12-13 days *in vitro*.

In vitro pharmacological treatment. For time-course experiments of sst2A receptor internalization, neurons were treated with 1 μM of the sst2A receptor agonist octreotide (OCT) in Neurobasal medium for 5, 10, 15 and 20 min at 37°C. For time-course experiments of sst2A receptor recycling, neurons were pretreated with 1 μM Ang IV (or PBS as control) in Neurobasal medium for 60 min at 37°C, followed by addition of 1 μM OCT or SRIF (Sigma-Aldrich) for 20 min. After rinsing, neurons were treated with 1 μM Ang IV (or PBS as control) in Neurobasal medium for 15, 30, 45, 60, 120 and 180 min at 37°C. Additional control conditions included neurons pretreated with 1 μM Ang IV (or PBS) without subsequent OCT or SRIF treatment (Control w/o OCT; Control w/o agonist). At the end of incubation times, neurons were fixed with 4% paraformaldehyde supplemented with 4% sucrose in PB for 20 min at RT.

shRNA lentiviral transduction. Rat IRAP expression was inhibited in cultured hippocampal cells using SMART vector 2.0 PGK-TurboGFP shRNA particles according to

manufacturer's protocols (Thermo Scientific, Dharmacon). Three predesigned individual IRAP-gene specific shRNA lentiviral particles were obtained from Dharmacon and provided as ready-to-use lentiviral particles (SH06-093146-01-10, SH06-093146-02-10 and SH06-093146-03-10). The shRNA target sequences were as follows: IRAP LV-shRNA1: GATTGCTACAAACGGGAAA, IRAP LV-shRNA2: AAGTTGGAGCAAGAACCGA and IRAP LV-shRNA3: GATTAGTGACCAGAGTACA. SMART vector 2.0 Non-targeting PGK-Turbo GFP particles (S06-0050000-01) was used as control (NT LV-shRNA; TGGTTTACATGTTGTGTGA). Hippocampal cells were transduced immediately after dissociation for 1 h at 37°C (at a multiplicity of infection-moi-of 10) and used for sst2A receptor recycling experiments at 12-13 days *in vitro*. Based on TurboGFP expression, neuronal efficiency of transduction was 38.3% for the IRAP LV-shRNA1, 32.3% for the IRAP LV-shRNA2, 49.1% for the IRAP LV-shRNA3 and 45.0% for the NT LV-shRNA.

Immunocytochemistry. Cells were washed in PBS and incubated 30 min in PBS with 5% NDS and 0.1% Triton X-100. Primary antibodies were diluted in PBS with 1% NDS and 0.1% Triton X-100 and incubated overnight at 4°C. Neurons were washed in PBS and subsequently incubated with secondary antibodies diluted in PBS with 1% NDS and 0.1 % Triton X-100 for 1 h at RT. Finally, coverslips were washed in PBS and mounted with Fluoromount (Southern Biotech) for confocal microscopic analysis.

Confocal microscopy. Immunofluorescent sections were analyzed using a Leica TCS SP8 confocal scanning system (Leica Microsystems) equipped with 488-nm Ar, 561-nm DPSS and 633-nm HeNe lasers or a Zeiss LSM 5 Exciter confocal scanning system (Carl Zeiss) with 488-nm Ar, 543-nm HeNe and 633-nm HeNe lasers. Eight-bit digital images were collected from a single optical plane using a 63x HC PL APO CS2 oil-immersion Leica objective (numerical aperture 1.40) or a 63x Plan-Apochromat oil-immersion Zeiss lens (numerical aperture 1.4). For

each optical section, double- or triple-fluorescence images were acquired in sequential mode to avoid potential contamination by linkage specific fluorescence emission cross-talk. Settings for laser intensity, beam expander, pinhole (1 Airy unit), range property of emission window, electronic zoom, gain and offset of photomultiplicator, field format, scanning speed were optimized initially and held constant throughout the study so that all sections were digitized under the same conditions.

Quantitative analysis of immunofluorescence. To assess the extent of IRAP knockdown, images of IRAP immunofluorescence from neuronal cell bodies were collected from a single optical plane using a 63x Plan-Apochromat oil-immersion Zeiss lens (numerical aperture 1.4). Images were segmented using identical threshold values, and integrated signal density was measured using the ImageJ software (Rasband, W.S., ImageJ, U. S. National Institutes of Health, Bethesda, Maryland, USA, http://imagej.nih.gov/ij/, 1997-2014.). This parameter, corresponding to the intensity of the immunofluorescence staining, was measured in an average of 30 neurons/group from 3 independent experiments. Mean values for the 4 experimental groups (IRAP LV-shRNA1-3 constructs and NT LV-shRNA control) were calculated and statistically analyzed.

To quantify sst2A receptor immunoreactivity at the plasma membrane, images of sst2A receptor and TGN38 immunofluorescence from neuronal cell bodies were acquired from a single optical plane using a 63x Plan-Apochromat oil-immersion Zeiss lens (numerical aperture 1.4). The z-axis level was selected where the TGN38-labeled *trans*-Golgi network was clearly identified and the sst2A receptor labeling at the plasma membrane was identified as a line-like ring in the green channel around the TGN38 labeling of the red channel (Fig. 6a). A 1 μm wide band containing the line-like sst2A receptor labeling was defined and the average pixel intensity, corresponding to the intensity of the immunofluorescent staining, was measured within the selection using the ImageJ software in an average of 30 neurons/group from 3 independent

experiments. Three sets of experiments were analyzed. One set contained 14 groups of the time-course experiments of sst2A receptor recycling (Control w/o OCT; 15, 30, 45, 60, 120 and 180 min after OCT washout with or without Ang IV). The second set contained 6 groups (Control w/o agonist; 45 min after OCT washout and 45 min after SRIF washout with or without Ang IV). The third set contained 4 groups of the lentiviral shRNA experiments (IRAP LV-shRNA1-3 constructs and NT LV-shRNA control; 45 min after OCT washout). Mean values for the experimental groups were calculated and statistically analyzed.

Binding of IRAP ligands to sst2A receptor in stably transfected CHO-K1 cells. Chinese Hamster Ovary (CHO-K1) cells stably transfected with the sst2A receptor were plated in 24-well plates (Becton Dickinson) and cultured until confluence in Dulbecco's modified essential medium (DMEM) supplemented with L-glutamine (2 mM), 2% (v/v) of a stock solution containing 5000 IU/ml penicillin and 5000 µg/ml streptomycine (Invitrogen), 1% (v/v) of a stock solution containing non-essential amino acids, 1 mM sodium pyruvate and 10% (v/v) fetal bovine serum (Invitrogen). Before the experiment, cells were washed twice with 500 µl per well of Krebs buffer (20 mM, $CaCl_2$, 2.7 mM KCl, 2.1 mM $MgCl_2$, 137 mM NaCl and 20 mM HEPES, pH 7.4) at RT. Incubations were carried out for 45 min at 37°C in a final volume of 500 µl per well consisting of 400 µl Krebs buffer, 50 µl of increasing concentrations of Ang IV or LVV-H7 (10^{-9} M – 10^{-5} M) and 50 µl ^{125}I-labeled SRIF (0.5 nM). At the end of the incubation period, the plates were placed on ice and washed three times with ice-cold PBS. For whole-cell binding (i.e. without distinction between surface-binding and intracellular accumulation of the radioligand) cells were then solubilized by addition of 300 µl NaOH (1 M). After 60 min treatment at RT, solutes were transferred in scintillation vials. Three ml of scintillation liquid (Optiphase Hisafe, Perkin Elmer) was added and the remaining radioactivity was measured in a γ-counter (Perkin Elmer). The experiments were repeated four times and results are shown in a compilation graph as the percentage of ^{125}I-labeled SRIF binding to sst2A receptors, in the presence of Ang IV or LVV-H7.

Focal pilocarpine-induced seizures in rats.

Surgery. Adult male Wistar rats (275-300 g) were anaesthetized with a mixture of ketamine and diazepam (start dose: 90:4.5 mg/kg), placed on a stereotaxic frame and implanted with a microdialysis guide cannula (CMA/12, CMA Microdialysis/AB) above the left (or right) hippocampus at flat skull coordinates: A -5.6 mm, L ±4.6 mm, V −4.6 mm relative to Bregma. For experiments with intrahippocampal electroencephalographic (EEG) recording, the guide cannula was customized by gluing an insulated electrode wire to the guide cannula and exposing it over a length of 0.5 mm beyond the tip of the guide cannula. The guide was secured to the skull with dental cement. For experiments with intrahippocampal EEG recordings, rats were s.c. implanted with a sterilized radiotelemetric transmitter (F20-EET, Data Sciences International) which was then subcutaneously tunneled to the intrahippocampal measuring electrode and the reference electrode which was attached to the skull with a stainless steel screw implanted 1 mm anterior of lambda. Postoperative analgesia was provided by s.c. ketoprofen (3mg/kg). A concentric microdialysis probe (3 mm length, CMA/12 Elite, CMA Microdialysis/AB) was inserted into the guide cannula. Following transfer of the animals to the microdialysis cage, the microdialysis probe was perfused with a modified Ringer's solution (147 mM NaCl, 4 mM KCl, 2.3 mM $CaCl_2$) at a flow rate of 2 µl/min using a CMA infusion pump (CMA120, CMA Microdialysis/AB). Rats had free access to food and water. Confirmation of unilateral probe placement was established at the end of each experiment on 50 µm brain slices prepared on a cryostat (Reichtert-Jung 1206, Cambridge Instruments).

Microdialysis and seizure severity assessment. All microdialysis experiments were performed on the day following surgery. A microdialysis flow rate of 2 µl/min was maintained throughout the pilocarpine experiments. Seizures were evoked by adding 10 mM pilocarpine to the perfusion liquid during two 20 min sampling periods. Animals were rated on a seizure severity scale based on Racine's scale which was adopted to include behavioral changes

observed in the focal pilocarpine model: (0) normal non-epileptic activity; (1) stereotypical mouth and facial movements, wet dog shakes; (2) head nodding, tremor, staring; (3) forelimb clonus, forelimb extension; (4) rearing, tonic-clonic activity; (5) falling (Meurs et al. 2008). The total seizure severity score (TSSS) was the sum of the highest seizure severity score (SSS) observed in each of the seven collection periods following the start of pilocarpine administration, and was used as a measure of seizure severity. Additional experiments were performed in rats implanted with an intrahippocampal EEG recording electrode and radiotelemetric transmitter. These rats were placed in a microdialysis bowl equipped with an EEG monitoring unit with radiotelemetric receiver (PhysioTel RPC-1, Data Sciences International) coupled to a Notocord-hem Evolution acquisition system (Notocord). The intrahippocampal EEG was sampled at 100 Hz during microdialysis sampling and the total EEG seizure duration and latency until the first EEG seizure was determined. The observed behavioral seizures were correlated to EEG seizures by linear regression analysis. Protocols differed between experimental groups as detailed below.

Effect of intra-hippocampal Ang IV and LVV-H7 in the focal pilocarpine model. Following the collection of 8 baseline samples 0 µM, 1 µM or 10 µM Ang IV or LVV-H7 were perfused through the microdialysis probe from the 9th sample collection period onwards. Pilocarpine was co-perfused at a concentration of 10 mM during the 13th and 14th sample collection periods. Hippocampal dialysate samples were subsequently collected for an additional 5 collection periods.

Involvement of the sst2A receptor in the anticonvulsive effects of Ang IV and LVV-H7. The involvement of the sst2A receptor in the observed effects of Ang IV and LVV-H7 was investigated in experiments with collection of 6 baseline samples, followed by perfusion of the microdialysis probe with 0.1 µM cyanamid 154806 (Sigma Aldrich) or 0.1 µM BIM-23627 (kindly provided by Dr. Michael D. Culler, Ipsen Pharma) from the 7th sample collection period onwards. From the 9th sample collection period onwards, 0 µM, 10 µM and 15 µM Ang IV or 10 µM LVV-H7 were added to the perfusion liquid. Pilocarpine was co-perfused at a concentration of 10 mM

during the 13th and 14th sample collection periods. Hippocampal dialysate samples were collected for an additional 5 collection periods.

Selectivity of the effects of Ang IV and LVV-H7 in the focal pilocarpine model. The involvement of the AT1 receptor in the observed effects of Ang IV and the involvement of the μ/κ opioid receptors in the anticonvulsant effects of LVV-H7 was investigated in experiments according to exactly the same microdialysis protocol as described above for the sst2A receptors. AT1 receptor antagonist candesartan and μ/κ opioid receptor antagonist naltrexone were used at 0.1 μM concentration.

Potentiation of the anticonvulsive effect of SRIF by Ang IV in the focal pilocarpine model. The effect of Ang IV on the anticonvulsive effect of SRIF was further investigated according to the previously described microdialysis protocol. Ang IV and SRIF were used in a subthreshold concentration that did not affect pilocarpine-induced seizures as such. Essentially we used 1 μM for Ang IV and 0.1 μM for SRIF. Ang IV and SRIF were perfused through the microdialysis probe, either alone or in combination, from the 9th sample collection period onwards. Pilocarpine was co-perfused at a concentration of 10 mM during the 13th and 14th sample collection periods. Hippocampal dialysate samples were subsequently collected for an additional 5 collection periods. Two rats treated with the combination of Ang IV and SRIF did not show EEG seizure activity and were excluded for analysis of EEG seizure latency.

Effects of IRAP ligands on rat hippocampal SRIF. Stereotactic surgery for bilateral probe implantation in left and right hippocampus was performed as described above for the unilateral intra-hippocampal probe implantation. Microdialysis probes (3 mm length, CMA/12 Elite, CMA Microdialysis/AB) were continuously perfused with artificial cerebrospinal fluid (aCSF, 125 mM NaCl, 2.5 mM KCl, 1.2 mM $CaCl_2$, 1.2 mM $MgCl_2$, 3.5 mM NaH_2PO_4, 0.2 mM ascorbic acid, 0.025% bovine serum albumin, pH 7.4) at a flow rate of 1.0 μl/min using a microdialysis pump

(CMA120, CMA Microdialysis/AB) following transfer of the animals to a microdialysis cage with free access to food and water. The day following surgery, samples from the two bilateral probes were collected every 30 min and pooled yielding a total volume of 60 µl. At the beginning of each experiment, samples were collected under baseline conditions, corresponding to perfusion of the probe with aCSF alone. Then 10 µM Ang IV or 10 µM LVV-H7 was added to the perfusion liquid for the remainder of the experiment. SRIF dialysate content was determined using a radioimmuno assay (RIA) with [^{125}I]-Tyr^{11}-Somatostatin (IM 161, Amersham) and a SRIF antibody (N 1611, Amersham) raised against cyclic SRIF. A standard curve was prepared using [^{125}I]-Tyr^{11}-somatostatin (6000 cpm, 2200 Ci/mmol), the antibody (final dilution 1/3000) and synthetic cyclic SRIF in a 0.8 ml solution containing 50 mM sodium phosphate, 10 mM EDTA and 0.3% bovine serum albumin (pH 7.4). The radioactivity was counted with a γ-counter. Results were read from the standard curve and the minimal detectable dose was 39.3 pg/100 µl. Confirmation of bilateral probe placement was again established at the end of each experiment on 50 µm brain slices prepared on a cryostat (Reichtert-Jung 1206, Cambridge Instruments).

Electron microscopy. For electron microscopic detection of the sst2A receptor in pilocarpine-treated rats in the presence or absence of Ang IV, a similar microdialysis protocol as described above under "*Effect of intra-hippocampal Ang IV and LVV-H7 in the focal pilocarpine model* " was used. However, after the 15th collection period (time point where maximal seizures are detected), rats were deeply anesthetized with sodium pentobarbital (60 mg/kg i.p.) and perfused through the ascending aorta with 100 ml of saline followed by 400 ml of ice-cold 4% paraformaldehyde and 0.05% glutaraldehyde in PB. Brains were post-fixed overnight in 4% paraformaldehyde at 4°C. Coronal sections were cut on a vibratome at 70 µm and collected in PBS. Sections within 1 mm of the microdialysis probe were selected and equilibrated in 25%

sucrose and 10% glycerol in 0.05 M PB, frozen rapidly in isopentane cooled in liquid nitrogen, and thawed in PBS at RT.

For pre-embedding immunocytochemistry, sections were preincubated for 30 min in 5% NGS in PBS. Sections were then incubated overnight at RT in rabbit anti-sst2A receptor antibody (1:1000) diluted in PBS containing 1% NGS. After washing in PBS, sections were incubated for 120 min in Nanogold®-conjugated goat anti rabbit IgG (1:100; Nanoprobes) diluted in PBS containing 2% of bovine serum albumin-c and 0.2% of cold water fish gelatin. Sections were washed in PBS and post-fixed in 1% glutaraldehyde in PBS for 10 min. After washings in PBS and 0.1 M sodium acetate buffer, pH 7.0, sst2A receptor immunogold labeling was intensified using a silver enhancement kit (HQ Silver; Nanoprobes) for 5-10 min in the dark at RT. After washings in acetate buffer and in PB, sections were post-fixed in 1% osmium tetroxide in PB for 10 min at RT. After washings in PB, they were dehydrated in an ascending series of ethanol, which included 1% uranyl acetate in 70% ethanol. They were then treated with propylene oxide twice for 10 min, equilibrated overnight in Durcupan ACM (Fluka), mounted on glass slides and cured at 60°C for 48 h. Areas of interest were cut out from the slide and glued to blank cylinders of resin. Blocks were cut in semithin sections (1 µm) and then in ultrathin sections on a Reichert Ultracut S microtome. Ultrathin sections were collected on pioloform-coated single-slot grids. Sections were stained with lead citrate and examined with a Philips CM120 electron microscope equipped with Morada Soft Imaging System (Olympus Soft Imaging Solutions). On the ultrathin sections, only areas at the surface of the vibratome sections were analyzed. The acquired images were equally adjusted for brightness and contrast, and composite illustrations were built in Adobe Photoshop CS3 (Adobe Systems).

Quantification of electron microscopic immunocytochemistry. The subcellular distribution of sst2A receptor in CA1 pyramidal cell dendrites was analyzed using the Measure command and Cell counter plugin of ImageJ in 3 control and 3 Ang IV-treated rats. An average of 10

dendrites per animal was analyzed. The length of the plasma membrane and the caliber of dendrites (expressed in cross-sectional surface; μm^2) were measured. The sst2A receptor immunoparticles were identified and counted in association with the plasma membrane and in the intracellular compartment. Results were expressed as: (1) the percentage of immunoparticles associated with the plasma membrane and the intracellular compartment (%); (2) density of immunoparticles per membrane length (μm) or cytoplasmic surface (μm^2).

Data analysis. Statistical analysis was performed using GraphPad Prism 4.0 (GraphPad Prism Software Inc.). Statistical tests applied to the data are indicated in the legends of the figures. Differences were considered to be significant at $p < 0.05$. All data in text and figures are presented as mean±S.E.M.

Results

Sst2A receptor-expressing neuronal cells colocalize with IRAP in the rat hippocampal formation

The sst2A receptor and IRAP display similar regional expression patterns (Fig. 1a,c). Whereas IRAP imunoreactivity was localized in the principal cells of CA1-3 and dentate gyrus (Fig. 1c,d), sst2A receptor immunoreactivity is distributed in both dendritic fields and principal cells of the hippocampus (Fig. 1a,d inset) (Csaba et al., 2001; Csaba et al., 2007). *In vivo* internalization of the receptor through intra-hippocampal octreotide (OCT) injections revealed sst2A receptor-expressing cell bodies (Fig. 1b,e), as previously reported (Csaba et al., 2001; Csaba et al., 2007). Double-labeling experiments demonstrated that all hippocampal sst2A receptor-positive neurons displayed IRAP immunoreactivity (Fig. 1e-g).

Internalized sst2A receptors are targeted to IRAP-positive vesicles in neurons

IRAP and sst2A receptor sub-cellular distribution was then studied in cultured rat hippocampal neurons to analyze whether both proteins could colocalize during receptor internalization and recycling. In non-treated control cells (Fig. 2), a predominant plasma membrane distribution of the endogenous sst2A receptor was detected at the surface of perikarya and dendrites, confirming our former results (Csaba et al., 2001; Csaba et al., 2007; Lelouvier et al., 2008). In accordance with earlier studies (Fernando et al., 2005; Fernando et al., 2007), endogenous IRAP immunoreactivity was mainly confined to intracytoplasmic granules in the perikarya and was also detected in proximal dendrites (Fig. 2). Finally, in the neuronal cell body, IRAP-positive vesicles were located in a perinuclear compartment and overlapped with the *trans*-Golgi marker TGN38, as previously reported (Fernando et al., 2007; Fernando et al., 2008) (Fig. 2). In agreement with these latter studies, a faint IRAP signal was also apparent at the

plasma membrane. Therefore, little colocalization between sst2A receptor and IRAP was observed in control conditions.

After 5-10 min of agonist stimulation with 1 µM OCT, endogenous sst2A receptors were no longer present at the cell surface, and bright fluorescent accumulations appeared in the cytoplasm of perikarya and dendrites (Fig. 2). The same redistribution of sst2A immunoreactivity was observed after 1 µM SRIF treatment (data not shown), as previously reported (Lelouvier et al., 2008). Very interestingly, extensive colocalization between sst2A receptor and IRAP immunoreactivity was detected both in perikarya and proximal dendrites between 5 and 20 min following the beginning of the OCT treatment, as shown by the yellow pseudocolor signal present in the overlaid images (Figs. 2, 3). This indicates that internalized receptors are massively targeted to IRAP-positive intracellular compartments in hippocampal neurons. This colocalization gradually decreased in time as the receptor recycled back to the plasma membrane (Fig. 4).

IRAP ligand accelerates sst2A receptor recycling in hippocampal neurons

Next, we performed kinetic experiments to analyze whether IRAP ligand Ang IV could impact on the trafficking and recycling of endogenous sst2A receptor following agonist-induced internalization (Fig. 5). In hippocampal neurons treated with OCT but in the absence of Ang IV, reappearance of sst2A receptors at the plasma membrane of the cell body was first evident 30 min after OCT washout. Three hours after OCT stimulation, receptor distribution and density were similar to control conditions, i.e. receptors were localized at the plasma membrane of both the cell body and dendrites.

In hippocampal neurons treated with OCT but in the presence of Ang IV, we observed a shift of the reappearance of the sst2A receptors at the plasma membrane (Figs. 5, 6). At 30, 45 and 60 min after OCT washout, the amount of membrane-associated receptors was significantly higher in Ang IV-treated neurons (OCT + Ang IV) than in respective controls (OCT + PBS) (30

min: +69%, 45 min: +82%, 60 min: +64%; Fig. 6b). No difference was observed in the recycling kinetics of the sst2A receptor following SRIF- or OCT-induced internalization. Notably, Ang IV treatment resulted in a faster sst2A receptor recycling with both agonists (Fig. 6b). Interestingly, within the Ang IV-treated group, we observed that 45 and 60 min after OCT washout the density of receptors at the plasma membrane was significantly higher than in cells not treated with OCT (Ang IV without OCT) (45 min: +33%, $p < 0.001$; 60 min: +18%, $p < 0.01$; Dunnett's Multiple Comparison Test; Fig. 6b). In cells treated with OCT in the absence of Ang IV, this phenomenon was also apparent but only 120 min after OCT washout (+16% vs. PBS without OCT, $p < 0.001$, Dunnett's Multiple Comparison Test; Fig. 6b). These data suggest that massive pools of sst2A receptors are first targeted from the perinuclear recycling compartment to the plasma membrane of the cell body, before diffusing to the dendritic fields along the membranes, and this process is accelerated in Ang IV-treated neurons. Together, these results suggest that the IRAP ligand has shortened the recycling time of internalized sst2A receptors to the plasma membrane.

IRAP ligands do not bind the sst2A receptor

To analyze whether the Ang IV effects on sst2A receptor recycling could be due to putative cross-reaction between the IRAP ligands and the sst2A receptor, cultured hippocampal neurons were treated with 1 µM Ang IV or LVV-H7 and fixed 20 to 180 min thereafter for immunoreactive detection of the endogenous sst2A receptor. Neither Ang IV nor LVV-H7 did change the distribution of sst2A receptor immunoreactivity (data not shown). The possible direct interaction between IRAP ligands and the sst2A receptor was also investigated in CHO-K1 cells stably transfected with the sst2A receptor incubated with increasing concentrations of Ang IV and LVV-H7. The total percentage of ^{125}I-labeled SRIF binding to sst2A receptor did not change throughout the whole experiment, in the presence of either Ang IV or LVV-H7 (Fig. 7). Together, these results indicate that direct interactions between IRAP ligands and sst2A receptors are unlikely.

IRAP knockdown also accelerates sst2A receptor recycling in hippocampal neurons

To confirm the specificity of IRAP effects on sst2A receptor trafficking, we next aimed to silence IRAP expression in hippocampal neurons through lentiviral-mediated RNA interference. The protein expression level of IRAP was analyzed by semi-quantitative laser scanning confocal microscopy in individual transduced neurons (Fig. 8a,b). Data revealed a significant inhibition of IRAP expression by 3 separate IRAP-targeting shRNAs as compared to control shRNA (IRAP LV-shRNA1: -76%, IRAP LV-shRNA2: -70%, IRAP shRNA3: -60%; Fig. 8b). This selective down-regulation of IRAP had no effect on the targeting of the sst2A receptor to the plasma membrane or on the capacity of the receptor to internalize after OCT stimulation. Importantly, when we analyzed the recycling of the receptor at the time point 45 min after OCT washout (Fig. 9a,b; chosen on the basis of pharmacological experiments for which the difference between Ang IV-treated and respective control neurons was the highest), we found that the density of the receptor at the plasma membrane was significantly higher in neurons transduced with IRAP-targeting shRNAs than in neurons transduced with control shRNA (IRAP LV-shRNA1: +56%, IRAP LV-shRNA2: +62%, IRAP shRNA3: +53%, Fig. 9b). These results suggest that reduction of IRAP expression has shortened the time of recycling of internalized receptors to the plasma membrane and that IRAP is therefore a negative regulator of sst2A receptor recycling.

Intra-hippocampal Ang IV or LVV-H7 administration is anticonvulsive in the rat focal pilocarpine model

To further analyze whether a faster recovery of internalized sst2A receptors at the plasma membrane in response to IRAP ligands could be relevant *in vivo*, we next studied the effects of intra-hippocampal administration of Ang IV and LVV-H7 in a rat model of focal seizures. Indeed, an increase in SRIF immunoreactivity and secretion is known to occur in

epileptic hippocampal tissues (Tallent and Qiu, 2008) and several studies argue for a concomitant internalization of the sst2A receptors (Csaba et al., 2004; Csaba et al., 2005).

Intra-hippocampal perfusion of 10 mM pilocarpine via a microdialysis probe induced a range of behavioral changes including wet dog shakes, typically beginning within 20 min following the start of pilocarpine administration. These changes progressively evolved into bouts of staring, stereotypical mouth and facial movements, forelimb clonus, and rearing. The behavioral changes correlated with electrocorticographic seizures, as previously demonstrated (Meurs et al., 2008). Pilocarpine-treated animals received intra-hippocampal co-perfusions of 1 or 10 µM of the IRAP ligands Ang IV or LVV-H7 through a microdialysis probe. The maximum seizure severity score (SSS) (Fig. 10a,b; Bin 12) of animals perfused with 1 µM Ang IV or 1 µM LVV-H7 was not significantly different from the maximum SSS of animals in the pilocarpine control group. Similarly, the mean total seizure severity score (TSSS) of animals treated with 1 µM Ang IV or 1 µM LVV-H7 were not significantly different from the mean TSSS observed in the pilocarpine control group. By contrast, the maximum SSS (Fig. 10a,b; Bin 12) for animals treated with 10 µM Ang IV or 10 µM LVV-H7 were significantly lower compared to the SSS in animals of the pilocarpine control group (Fig. 10a,b). In animals treated with 10 µM Ang IV or 10 µM LVV-H7, only minor seizure-related behavioral changes were observed, such as wet dog shakes and less commonly staring. Correspondingly, the mean TSSS of animals treated with 10 µM Ang IV or 10 µM LVV-H7 were significantly lower compared to the mean TSSS observed in the pilocarpine control group (Fig. 10a,b). Taken together, these results demonstrate that IRAP ligands, at a microdialysis probe perfusion concentration of 10 µM, display anticonvulsant effects.

The anticonvulsant effects of IRAP ligands are mediated by the sst2A receptor

To further analyze whether the anticonvulsant properties of IRAP could be mediated by the sst2A receptor, we next studied the effect of intra-hippocampal co-administration of sst2A

receptor antagonists and IRAP ligands in the same limbic seizure model. The sst2A receptor antagonists cyanamid 154806 or BIM-23627 did not significantly affect seizure severity compared to the pilocarpine control groups when perfused in the hippocampus at a concentration of 0.1 μM (Fig. 11a,b). However, seizure severity was significantly higher in animals perfused with 0.1 μM cyanamid 154806 followed by 10 μM Ang IV (Fig. 11a) or 10 μM LVV-H7 (Fig. 11c) and 0.1 μM BIM-23627 followed by 15 μM Ang IV (Fig. 11b) compared to Ang IV and LVV-H7 alone (Fig. 11a-c). Altogether, these experiments demonstrate that sst2A receptor antagonists abolish the anticonvulsant effects of Ang IV and LVV-H7 and that the sst2A receptor is thus a key factor for the anticonvulsant effects mediated by the IRAP ligands.

The anticonvulsant effects of IRAP ligands are independent of angiotensin AT1 and μ/κ opioid receptor activation

Because Ang IV and LVV-H7 were previously characterized as low affinity angiotensin AT1 (Yang et al., 2008; De Bundel et al., 2009; De Bundel et al. 2010) and opioid μ/κ receptor (Zhao et al., 1997; Lee et al., 2001) agonists, we therefore investigated the possible involvement of these receptor subtypes in the anticonvulsant effects of Ang IV and LVV-H7. The angiotensin AT1 receptor antagonist candesartan and the opioid μ/κ receptor antagonist naltrexone, perfused into the hippocampus at a concentration of 0.1 μM, had no significant effect on seizure severity compared to the pilocarpine control group (Fig. 12a,b). Furthermore, pre-treatment with candesartan or naltrexone did not abolish the anticonvulsive effect of Ang IV and LVV-H7 as compared to the pilocarpine control group (Fig. 12a,b).

IRAP ligands have no effect on extracellular hippocampal SRIF levels

Anticonvulsant effects of IRAP ligands could be due, in addition to their effects on sst2A receptor recycling, to an increase in hippocampal SRIF concentrations through inhibition of its degradation, as reported in one *in vitro* study in PC12 cells (Matsumoto et al., 2001). We

563 therefore analyzed the effects of intra-hippocampal administration of anticonvulsant
564 concentrations of Ang IV or LVV-H7 on hippocampal SRIF levels. The mean baseline
565 concentrations of SRIF in hippocampal microdialysates was 0.80±0.15 nM. Intra-hippocampal
566 perfusion of 10 µM Ang IV or 10 µM LVV-H7 had no effect on baseline SRIF levels of the
567 hippocampal microdialysates (Fig. 13). The inhibition of enzymatic SRIF degradation is therefore
568 not implicated in the mechanism of anticonvulsant action of the IRAP ligands.
569
570 ***Ang IV potentiates the anticonvulsive effect of SRIF***
571 We next investigated whether intrahippocampal administration of the IRAP ligand Ang IV could
572 potentiate the anticonvulsive effect of SRIF (Aourz et al., 2011). We found that 1 µM Ang IV and
573 0.1 µM SRIF had no effect on pilocarpine-induced seizures. Co-perfusion of both peptides in the
574 same concentration suppressed behavioral seizures (Fig 14a) and EEG seizures (Fig 14b-g).
575 These data clearly demonstrate that Ang IV potentiates the anticonvulsive effect of SRIF in the
576 focal pilocarpine model, potentially by increasing the availability of sst2A receptors at the
577 membrane of hippocampal neurons.
578
579 ***IRAP ligands increase the density of membrane-associated sst2A receptors in vivo***
580 ***following evocation of a limbic seizure event***
581 To further demonstrate that Ang IV antiepileptic effects are driven by an increase of
582 membrane-associated receptors *in vivo*, as demonstrated *in vitro*, the density of sst2A receptors
583 was quantified by immunogold electron microscopy in CA1 pyramidal cell dendrites of
584 pilocarpine-injected animals treated or not with an anticonvulsive dose of Ang IV (Fig. 15a-d).
585 Whereas in the pilocarpine control group, 70% of immunoparticles were found in intracellular
586 compartments and 30% membrane-associated (Fig. 15a,c), in the animals receiving intra-
587 hippocampal perfusion of Ang IV and pilocarpine, the distribution was reversed: 30% of
588 immunoparticles were intracellular and 70% membrane-associated (Fig. 15b,c). The latter

589 distribution is close to that we have previously reported in naive animals, i.e. 20% intracellular
590 and 80% membrane-associated (Csaba et al., 2007). Quantitative analysis revealed that the
591 density of sst2A receptors at the plasma membrane was significantly higher in Ang IV-treated
592 animals as compared to controls (Fig. 15d). Conversely, the density of intracellular sst2A
593 receptor immunoparticles was significantly lower in Ang IV-treated animals as compared to
594 controls (Fig. 15d). These results suggest that, as demonstrated *in vitro*, Ang IV accelerates the
595 recycling of internalized receptors induced by SRIF release during the evoked seizure process.
596 Together with the fact that sst2A receptor antagonists prevent the anticonvulsive effects
597 mediated by Ang IV or LVV-H7, the recovery of the sst2A receptors at the plasma membrane
598 appears as the key mechanism involved in the anticonvulsive effects mediated by IRAP ligands.
599

Discussion

The life cycle of GPCRs includes biosynthesis in the endoplasmic reticulum, maturation in the Golgi and transport to the cell surface followed by signal transduction at the plasma membrane and often internalization. Additional signaling can also occur in early endosomes as recently demonstrated (Irannejad et al., 2013). GPCR-interacting proteins have been demonstrated to play a critical role along these different phases (von Zastrow and Williams, 2012). However, much remains to be learnt about mechanisms that regulate post-endocytic sorting and recycling of GPCRs. As documented in our study, the insulin-regulated aminopeptidase, IRAP, appears as a new modulator of GPCR trafficking by affecting the kinetics of the sst2A receptor recycling after ligand activation in neurons. *Trans*-modulation of the recycling of a GPCR through ligand binding to a non-GPCR membrane protein, has, to our knowledge, not yet been described. *Trans*-effects on GPCR trafficking were until now only described through oligomerization of receptors (von Zastrow and Williams, 2012), which mostly affect the endocytosis process. Importantly, our study also demonstrates that modulating the recycling of a particular receptor can indeed impact its physiological fate and therefore present a potential therapeutic value.

Within the hippocampus, the major SRIF receptor subtype, the sst2A receptor, is localized at post-synaptic sites of the principal cells (Dournaud et al., 1996; Schindler et al., 1997; Csaba et al., 2007). Although this receptor appears to be an attractive therapeutic target in epilepsy, it rapidly internalizes *in vivo* before a slow recycling process (Csaba et al., 2007; Lelouvier et al., 2008). This long route has been suggested to have an impact on sst2A receptor-mediated signaling when, in pathophysiological conditions such as epilepsy, a high and chronic release of SRIF occurs (Vezzani and Hoyer, 1999). Indeed, a decreased density of this receptor subtype has been demonstrated in both rat and human epileptic dentate gyrus (Csaba et al., 2004; Csaba et al., 2005). Importantly, our present data suggest that down-regulation of the

sst2A receptor can be counteracted and consequently can increase endogenous SRIF anticonvulsant properties. We first found that internalized receptors travel massively through an intra-cytoplasmic pool of IRAP-positive vesicles. IRAP has been proposed to serve as a cargo of cell-specific storage vesicles and as an active player in their trafficking (Saveanu and van Endert, 2012). Our findings support this notion since we demonstrate here that IRAP regulates either directly or indirectly the sorting of sst2A receptors from cytoplasmic vesicles to the plasma membrane. Secondly, we established that the IRAP ligand Ang IV or the knockdown of IRAP expression both accelerate the recycling of sst2A receptors after their endocytosis in hippocampal cells. These observations suggest a possible *trans*-modulation of sst2A receptor trafficking by IRAP. We then showed that the anticonvulsive effects of both Ang IV and the structurally distinct peptidergic IRAP ligand LVV-H7 were reversed by intra-hippocampal co-administration of two structurally different sst2A receptor antagonists, cyanamid 154806 and BIM-23627. These results unequivocally confirm the involvement of the sst2A receptor in the anticonvulsive effects of the IRAP ligands. Moreover, we found that a low dose of Ang IV, which does not exert anticonvulsive effects as such, potentiates the anticonvulsive action of SRIF. We then asked whether Ang IV and LVV-H7 may exert their anticonvulsive effects through putative inhibition of SRIF degradation via IRAP (Matsumoto et al., 2001). We have established that perfusion of anticonvulsive concentrations of Ang IV or LVV-H7 into the hippocampus had no effect on local SRIF levels. This suggests that IRAP is not involved in SRIF degradation in the rodent brain. Other enzymes, such as endopeptidase-24.11 (Sakurada et al., 1990; Barnes et al., 1995) or endopeptidase-24.15 and 24.16 (Dahms and Mentlein, 1992), may be more important for SRIF degradation. Consequently, we rule out the “enzyme hypothesis” as a mechanism of action in our limbic seizure model. Importantly, using immunogold electron microscopy, we further demonstrate that Ang IV increased *in vivo* the availability of membrane-associated sst2A receptors. Taken together, our results bring us to the conclusion that IRAP ligands favor a rapid recycling and resensitization of sst2A receptors following their

internalization and enhance endogenous SRIF inhibitory effects on seizure activity by increasing the density of functional receptors at the plasma membrane. These results are in agreement with studies using the ß2 adrenergic receptor (Pippig et al., 1995; Vistein and Puthenveedu, 2013) or the Human G Protein-Coupled Receptor 17 (Daniele et al., 2011) demonstrating that recycled receptors resensitize rapidly.

In the hippocampal formation, SRIF interneurons and the sst2A receptor, which is highly expressed in the dendritic fields of granular and pyramidal cells, are well poised to regulate neuronal hyperexcitability (Johansson et al., 1984; Tallent and Qiu, 2008). Hilar SRIF inhibitory interneurons and their axons that terminate on the distal dendrites of granule cells are positioned to inhibit granule cells at the perforant path inputs, a major excitatory pathway to the hippocampus. SRIF fibers are present in the hilus, suggesting that SRIF neurons also modulate hilar neurons (Leranth et al., 1990; Lubke et al., 1998). SRIF axons are also localized throughout the CA1-CA3 regions, being enriched in stratum lacunosum moleculare (Johansson et al., 1984). Distinct inhibitory actions at the cellular level in rat CA1 pyramidal neurons were demonstrated for SRIF. It increases two different types of K+ currents, the voltage-sensitive M-current (Moore et al., 1988; Schweitzer et al., 1990) and a voltage-insensitive leak current (Schweitzer et al., 1998). Postsynaptic hyperpolarization and reduced excitatory postsynaptic currents of CA1-3 pyramidal neurons by SRIF have also been reported (Tallent and Siggins, 1997, 1999). Taken together, these studies and our present results emphasize the importance of the hippocampal somatostatinergic network, which includes the availability of functional sst2A receptors at the plasma membrane for dampening neuronal hyperexcitability.

Although beyond the scope of the present study, it would be of interest to decipher the mechanisms by which IRAP is able to regulate the recycling of the sst2A receptor. In CHO-K1 and HEK 293 cells, iodinated Ang IV induced internalization of IRAP which appears to be clathrin-mediated (Demaegdt et al., 2008). Ligand-induced internalization and recycling of IRAP has also been suggested in neurons (Fernando et al., 2008). In hippocampal cells treated with

678 Ang IV, we did not observe a time-dependent accumulation of IRAP immunoreactivity within
679 intracytoplasmic vesicles. This suggests that intracellular stores of IRAP are constantly driven to
680 the cell surface to replace internalized IRAP, and that the IRAP exocytosis rate is higher in the
681 presence of its ligands. Because internalized sst2A receptors travel through IRAP-containing
682 vesicles, one can hypothesize that the rate of receptor exocytosis is indirectly dependent upon
683 the presence of IRAP ligands, i.e. sst2A receptors recycle faster in cells or tissue incubated with
684 Ang IV or LVV-H7. If this is the case, effects of IRAP ligands would not be specific for the sst2A
685 receptor but could also modulate other types of receptors that internalize and recycle through an
686 IRAP/TGN compartment. Most interestingly, Ang IV has been shown to reverse the kindling-
687 induced down-regulation of dopaminergic D1 and D2 receptors in the basal ganglia
688 (Tchekalarova et al., 2004), two receptors which are well known to internalize in neurons
689 (Dumartin et al., 1998; Skinbjerg et al., 2010; Lane et al., 2012). Thus IRAP ligands, in addition
690 to their potential for modulating limbic seizures, might also represent appealing therapeutic tools
691 in neurological diseases or following pharmacological treatments in which down-regulation of
692 GPCRs could occur (Bezard et al., 2001; Gainetdinov et al., 2004; Williams et al., 2013).
693 Although the above described mechanism by which IRAP ligands could impact on sst2A
694 receptor intracellular trafficking is a likely starting hypothesis, the cellular events involved could
695 be difficult to decipher. In insulin-sensitive cells, IRAP trafficking itself is far from being
696 understood, despite a large number of studies (Albiston et al., 2007). In addition, IRAP and the
697 sst2A receptor both interact through their intra-cytoplasmic domain with several proteins
698 involved in vesicle trafficking, tethering and membrane anchoring (Albiston et al., 2007; Watson
699 et al., 2008; Csaba et al., 2012). Interestingly, IRAP knockdown in adipocytes increase plasma
700 membrane GLUT4 levels due to increase of exocytosis (Jordens et al., 2010). Regarding our
701 present results showing that IRAP knockdown increases the recycling of the receptor to the
702 plasma membrane, it appears that IRAP could be a negative regulator of the exocytosis pathway

703 in different cell types. Further studies in neuronal cells are mandatory to shed lights on the
704 molecular and cellular mechanisms implicated in this process.

705 In conclusion, the present study demonstrates that two structurally different peptidergic
706 IRAP ligands protect against limbic seizures in rats. These anticonvulsive effects do not result
707 from the inhibition of the enzymatic activity of IRAP and subsequent prevention of SRIF
708 degradation. We demonstrate that IRAP, following ligand binding, *trans*-regulates the recycling
709 process of the sst2A receptor and increases the availability of this inhibitory receptor at the
710 plasma membrane. This represents a novel mechanism by which GPCR transmission can be
711 regulated and further demonstrates that IRAP is a potential therapeutic target for the treatment
712 of epilepsy. Whether IRAP could modulate the down-regulation of other types of GPCRs, thus
713 displaying additional therapeutic interests, will represent intriguing issues for future studies.

Acknowledgements

This work was supported by the Inserm (PG and PD), Paris Diderot University (PG and PD), La Fondation pour la Recherche sur le Cerveau (PD), the PremUP Foundation (PG), the Seventh Framework Program of the European Union (grant agreement No. HEALTH-F2-2009-241778/Neurobid, PG), the Assistance Publique-Hôpitaux de Paris (Contrat de Recherche Translationnelle, PD, PG and Contrat de Recherche Hospitalier, SA), the Fund for Scientific Research FWO Flanders (IS, grant G.0165.08 ; grant G.0163.10N), the Queen Elisabeth Medical Foundation GSKE (IS) and the Research Council of the Vrije Universiteit Brussel (IS, DD, OZR1943, OZR1443, GOA61). SP was supported by grants from the MRC. G.L.C. is a WCU (World Class University) International Scholar and supported by the WCU program through the KOSEF (Korea Science and Engineering Foundation), funded by the MEST (Korean Ministry of Education, Science and Technology) (R31-10089). We thank A. Rouche (Inserm U974, Institut de Myologie, Hôpital Pitié-Salpêtrière, Paris, France) for electron microscopy facilities. We thank G. De Smet for excellent technical assistance with microdialysis experiments and intrahippocampal EEG recordings.

Competing financial interests: The authors declare no competing financial interests.

References

Albiston AL, Mustafa T, McDowall SG, Mendelsohn FA, Lee J, Chai SY (2003) AT4 receptor is insulin-regulated membrane aminopeptidase: potential mechanisms of memory enhancement. Trends Endocrinol Metab 14:72-77.

Albiston AL, Peck GR, Yeatman HR, Fernando R, Ye S, Chai SY (2007) Therapeutic targeting of insulin-regulated aminopeptidase: heads and tails? Pharmacol Ther 116:417-427.

Albiston AL, Diwakarla S, Fernando RN, Mountford SJ, Yeatman HR, Morgan B, Pham V, Holien JK, Parker MW, Thompson PE, Chai SY (2011) Identification and development of specific inhibitors for insulin-regulated aminopeptidase as a new class of cognitive enhancers. Br J Pharmacol 164:37-47.

Aourz N, De Bundel D, Stragier B, Clinckers R, Portelli J, Michotte Y, Smolders I (2011) Rat hippocampal somatostatin sst3 and sst4 receptors mediate anticonvulsive effects in vivo: indications of functional interactions with sst2 receptors. Neuropharmacology 61:1327-1333.

Barnes K, Doherty S, Turner AJ (1995) Endopeptidase-24.11 is the integral membrane peptidase initiating degradation of somatostatin in the hippocampus. J Neurochem 64:1826-1832.

Bassant MH, Simon A, Poindessous-Jazat F, Csaba Z, Epelbaum J, Dournaud P (2005) Medial septal GABAergic neurons express the somatostatin sst2A receptor: functional consequences on unit firing and hippocampal theta. J Neurosci 25:2032-2041.

Bezard E, Brotchie JM, Gross CE (2001) Pathophysiology of levodopa-induced dyskinesia: potential for new therapies. Nat Rev Neurosci 2:577-588.

Chai SY, Fernando R, Peck G, Ye SY, Mendelsohn FA, Jenkins TA, Albiston AL (2004) The angiotensin IV/AT4 receptor. Cell Mol Life Sci 61:2728-2737.

762 Clynen E, Swijsen A, Raijmakers M, Hoogland G, Rigo JM (2014) Neuropeptides as targets for
763 the development of anticonvulsant drugs. Mol Neurobiol 50:626-646.
764 Csaba Z, Peineau S, Dournaud P (2012) Molecular mechanisms of somatostatin receptor
765 trafficking. J Mol Endocrinol 48:R1-12.
766 Csaba Z, Simon A, Helboe L, Epelbaum J, Dournaud P (2003) Targeting sst2A receptor-
767 expressing cells in the rat hypothalamus through in vivo agonist stimulation:
768 neuroanatomical evidence for a major role of this subtype in mediating somatostatin
769 functions. Endocrinology 144:1564-1573.
770 Csaba Z, Richichi C, Bernard V, Epelbaum J, Vezzani A, Dournaud P (2004) Plasticity of
771 somatostatin and somatostatin sst2A receptors in the rat dentate gyrus during kindling
772 epileptogenesis. Eur J Neurosci 19:2531-2538.
773 Csaba Z, Bernard V, Helboe L, Bluet-Pajot MT, Bloch B, Epelbaum J, Dournaud P (2001) In vivo
774 internalization of the somatostatin sst2A receptor in rat brain: evidence for translocation
775 of cell-surface receptors into the endosomal recycling pathway. Mol Cell Neurosci
776 17:646-661.
777 Csaba Z, Lelouvier B, Viollet C, El Ghouzzi V, Toyama K, Videau C, Bernard V, Dournaud P
778 (2007) Activated somatostatin type 2 receptors traffic in vivo in central neurons from
779 dendrites to the trans Golgi before recycling. Traffic 8:820-834.
780 Csaba Z, Pirker S, Lelouvier B, Simon A, Videau C, Epelbaum J, Czech T, Baumgartner C,
781 Sperk G, Dournaud P (2005) Somatostatin receptor type 2 undergoes plastic changes in
782 the human epileptic dentate gyrus. J Neuropathol Exp Neurol 64:956-969.
783 Dahms P, Mentlein R (1992) Purification of the main somatostatin-degrading proteases from rat
784 and pig brains, their action on other neuropeptides, and their identification as
785 endopeptidases 24.15 and 24.16. Eur J Biochem 208:145-154.
786 Daniele S, Trincavelli ML, Gabelloni P, Lecca D, Rosa P, Abbracchio MP, Martini C (2011)
787 Agonist-induced desensitization/resensitization of human G protein-coupled receptor 17:

a functional cross-talk between purinergic and cysteinyl-leukotriene ligands. J Pharmacol Exp Ther 338:559-567.

De Bundel D, Smolders I, Yang R, Albiston AL, Michotte Y, Chai SY (2009) Angiotensin IV and LVV-haemorphin 7 enhance spatial working memory in rats: effects on hippocampal glucose levels and blood flow. Neurobiol Learn Mem 92:19-26.

De Bundel D, Demaegdt H, Lahoutte T, Caveliers V, Kersemans K, Ceulemans AG, Vauquelin G, Vanderheyden P, Michotte Y, Smolders I (2010) Involvement of the AT1 receptor subtype in the effects of angiotensin IV and LVV-haemorphin 7 on hippocampal neurotransmitter levels and spatial working memory. J Neurochem 112:1223-1234.

Demaegdt H, Smitz L, De Backer JP, Le MT, Bauwens M, Szemenyei E, Toth G, Michotte Y, Vanderheyden P, Vauquelin G (2008) Translocation of the insulin-regulated aminopeptidase to the cell surface: detection by radioligand binding. Br J Pharmacol 154:872-881.

Dobolyi A, Kekesi KA, Juhasz G, Szekely AD, Lovas G, Kovacs Z (2014) Receptors of peptides as therapeutic targets in epilepsy research. Curr Med Chem 21:764-787.

Dournaud P, Boudin H, Schonbrunn A, Tannenbaum GS, Beaudet A (1998) Interrelationships between somatostatin sst2A receptors and somatostatin-containing axons in rat brain: evidence for regulation of cell surface receptors by endogenous somatostatin. J Neurosci 18:1056-1071.

Dournaud P, Gu YZ, Schonbrunn A, Mazella J, Tannenbaum GS, Beaudet A (1996) Localization of the somatostatin receptor SST2A in rat brain using a specific anti-peptide antibody. J Neurosci 16:4468-4478.

Dumartin B, Caille I, Gonon F, Bloch B (1998) Internalization of D1 dopamine receptor in striatal neurons in vivo as evidence of activation by dopamine agonists. J Neurosci 18:1650-1661.

Fernando RN, Albiston AL, Chai SY (2008) The insulin-regulated aminopeptidase IRAP is colocalised with GLUT4 in the mouse hippocampus--potential role in modulation of glucose uptake in neurones? Eur J Neurosci 28:588-598.

Fernando RN, Larm J, Albiston AL, Chai SY (2005) Distribution and cellular localization of insulin-regulated aminopeptidase in the rat central nervous system. J Comp Neurol 487:372-390.

Fernando RN, Luff SE, Albiston AL, Chai SY (2007) Sub-cellular localization of insulin-regulated membrane aminopeptidase, IRAP to vesicles in neurons. J Neurochem 102:967-976.

Gainetdinov RR, Premont RT, Bohn LM, Lefkowitz RJ, Caron MG (2004) Desensitization of G protein-coupled receptors and neuronal functions. Annu Rev Neurosci 27:107-144.

Irannejad R, Tomshine JC, Tomshine JR, Chevalier M, Mahoney JP, Steyaert J, Rasmussen SG, Sunahara RK, El-Samad H, Huang B, von Zastrow M (2013) Conformational biosensors reveal GPCR signalling from endosomes. Nature 495:534-538.

Johansson O, Hokfelt T, Elde RP (1984) Immunohistochemical distribution of somatostatin-like immunoreactivity in the central nervous system of the adult rat. Neuroscience 13:265-339.

Jordens I, Molle D, Xiong W, Keller SR, McGraw TE (2010) Insulin-regulated aminopeptidase is a key regulator of GLUT4 trafficking by controlling the sorting of GLUT4 from endosomes to specialized insulin-regulated vesicles. Mol Biol Cell 21:2034-2044.

Keller SR (2003) The insulin-regulated aminopeptidase: a companion and regulator of GLUT4. Front Biosci 8:s410-420.

Lane DA, Chan J, Fitzgerald ML, Kearn CS, Mackie K, Pickel VM (2012) Quinpirole elicits differential in vivo changes in the pre- and postsynaptic distributions of dopamine D(2) receptors in mouse striatum: relation to cannabinoid-1 (CB(1)) receptor targeting. Psychopharmacology (Berl) 221:101-113.

838 Lee J, Chai SY, Mendelsohn FA, Morris MJ, Allen AM (2001) Potentiation of cholinergic
839 transmission in the rat hippocampus by angiotensin IV and LVV-hemorphin-7.
840 Neuropharmacology 40:618-623.
841 Lelouvier B, Tamagno G, Kaindl AM, Roland A, Lelievre V, Le Verche V, Loudes C, Gressens P,
842 Faivre-Baumann A, Lenkei Z, Dournaud P (2008) Dynamics of somatostatin type 2A
843 receptor cargoes in living hippocampal neurons. J Neurosci 28:4336-4349.
844 Leranth C, Malcolm AJ, Frotscher M (1990) Afferent and efferent synaptic connections of
845 somatostatin-immunoreactive neurons in the rat fascia dentata. J Comp Neurol 295:111-
846 122.
847 Leto D, Saltiel AR (2012) Regulation of glucose transport by insulin: traffic control of GLUT4. Nat
848 Rev Mol Cell Biol 13:383-396.
849 Loyens E, Schallier A, Chai SY, De Bundel D, Vanderheyden P, Michotte Y, Smolders I (2011)
850 Deletion of insulin-regulated aminopeptidase in mice decreases susceptibility to
851 pentylenetetrazol-induced generalized seizures. Seizure 20:602-605.
852 Lubke J, Frotscher M, Spruston N (1998) Specialized electrophysiological properties of
853 anatomically identified neurons in the hilar region of the rat fascia dentata. J
854 Neurophysiol 79:1518-1534.
855 Matsumoto H, Nagasaka T, Hattori A, Rogi T, Tsuruoka N, Mizutani S, Tsujimoto M (2001)
856 Expression of placental leucine aminopeptidase/oxytocinase in neuronal cells and its
857 action on neuronal peptides. Eur J Biochem 268:3259-3266.
858 Meurs A, Clinckers R, Ebinger G, Michotte Y, Smolders I (2008) Seizure activity and changes in
859 hippocampal extracellular glutamate, GABA, dopamine and serotonin. Epilepsy Res
860 78:50-59.
861 Moore SD, Madamba SG, Joels M, Siggins GR (1988) Somatostatin augments the M-current in
862 hippocampal neurons. Science 239:278-280.

863 Olias G, Viollet C, Kusserow H, Epelbaum J, Meyerhof W (2004) Regulation and function of
864 somatostatin receptors. J Neurochem 89:1057-1091.
865 Peineau S, Potier B, Petit F, Dournaud P, Epelbaum J, Gardette R (2003) AMPA-sst2
866 somatostatin receptor interaction in rat hypothalamus requires activation of NMDA and/or
867 metabotropic glutamate receptors and depends on intracellular calcium. J Physiol
868 546:101-117.
869 Pippig S, Andexinger S, Lohse MJ (1995) Sequestration and recycling of beta 2-adrenergic
870 receptors permit receptor resensitization. Mol Pharmacol 47:666-676.
871 Sakurada C, Yokosawa H, Ishii S (1990) The degradation of somatostatin by synaptic
872 membrane of rat hippocampus is initiated by endopeptidase-24.11. Peptides 11:287-292.
873 Saveanu L, van Endert P (2012) The role of insulin-regulated aminopeptidase in MHC class I
874 antigen presentation. Front Immunol 3:57.
875 Schindler M, Sellers LA, Humphrey PP, Emson PC (1997) Immunohistochemical localization of
876 the somatostatin SST2(A) receptor in the rat brain and spinal cord. Neuroscience 76:225-
877 240.
878 Schweitzer P, Madamba S, Siggins GR (1990) Arachidonic acid metabolites as mediators of
879 somatostatin-induced increase of neuronal M-current. Nature 346:464-467.
880 Schweitzer P, Madamba SG, Siggins GR (1998) Somatostatin increases a voltage-insensitive
881 K+ conductance in rat CA1 hippocampal neurons. J Neurophysiol 79:1230-1238.
882 Skinbjerg M, Liow JS, Seneca N, Hong J, Lu S, Thorsell A, Heilig M, Pike VW, Halldin C, Sibley
883 DR, Innis RB (2010) D2 dopamine receptor internalization prolongs the decrease of
884 radioligand binding after amphetamine: a PET study in a receptor internalization-deficient
885 mouse model. Neuroimage 50:1402-1407.
886 Stragier B, Clinckers R, Meurs A, De Bundel D, Sarre S, Ebinger G, Michotte Y, Smolders I
887 (2006) Involvement of the somatostatin-2 receptor in the anti-convulsant effect of

angiotensin IV against pilocarpine-induced limbic seizures in rats. J Neurochem 98:1100-1113.

Stumm RK, Zhou C, Schulz S, Endres M, Kronenberg G, Allen JP, Tulipano G, Hollt V (2004) Somatostatin receptor 2 is activated in cortical neurons and contributes to neurodegeneration after focal ischemia. J Neurosci 24:11404-11415.

Tallent MK, Siggins GR (1997) Somatostatin depresses excitatory but not inhibitory neurotransmission in rat CA1 hippocampus. J Neurophysiol 78:3008-3018.

Tallent MK, Siggins GR (1999) Somatostatin acts in CA1 and CA3 to reduce hippocampal epileptiform activity. J Neurophysiol 81:1626-1635.

Tallent MK, Qiu C (2008) Somatostatin: an endogenous antiepileptic. Mol Cell Endocrinol 286:96-103.

Tchekalarova J, Kambourova T, Georgiev V (2001) Effects of angiotensin III and angiotensin IV on pentylenetetrazol seizure susceptibility (threshold and kindling): interaction with adenosine A(1) receptors. Brain Res Bull 56:87-91.

Tchekalarova J, Sotiriou E, Angelatou F (2004) Down-regulation of dopamine D1 and D2 receptors in the basal ganglia of PTZ kindling model of epilepsy: effects of angiotensin IV. Brain Res 1024:159-166.

Vanderheyden PM (2009) From angiotensin IV binding site to AT4 receptor. Mol Cell Endocrinol 302:159-166.

Vezzani A, Hoyer D (1999) Brain somatostatin: a candidate inhibitory role in seizures and epileptogenesis. Eur J Neurosci 11:3767-3776.

Vistein R, Puthenveedu MA (2013) Reprogramming of G protein-coupled receptor recycling and signaling by a kinase switch. Proc Natl Acad Sci U S A 110:15289-15294.

von Zastrow M, Williams JT (2012) Modulating neuromodulation by receptor membrane traffic in the endocytic pathway. Neuron 76:22-32.

913 Watson RT, Hou JC, Pessin JE (2008) Recycling of IRAP from the plasma membrane back to
914 the insulin-responsive compartment requires the Q-SNARE syntaxin 6 but not the GGA
915 clathrin adaptors. J Cell Sci 121:1243-1251.
916 Williams JT, Ingram SL, Henderson G, Chavkin C, von Zastrow M, Schulz S, Koch T, Evans CJ,
917 Christie MJ (2013) Regulation of mu-opioid receptors: desensitization, phosphorylation,
918 internalization, and tolerance. Pharmacol Rev 65:223-254.
919 Wright JW, Harding JW (2011) Brain renin-angiotensin--a new look at an old system. Prog
920 Neurobiol 95:49-67.
921 Yang R, Smolders I, De Bundel D, Fouyn R, Halberg M, Demaegdt H, Vanderheyden P, Dupont
922 AG (2008) Brain and peripheral angiotensin II type 1 receptors mediate renal
923 vasoconstrictor and blood pressure responses to angiotensin IV in the rat. J Hypertens
924 26:998-1007.
925 Zhao Q, Garreau I, Sannier F, Piot JM (1997) Opioid peptides derived from hemoglobin:
926 hemorphins. Biopolymers 43:75-98.
927
928

Legends

Figure 1. Neurons expressing the sst2A receptor also display IRAP immunoreactivity in the rat hippocampal formation. a) In control rats, diffuse sst2A receptor immunoreactivity is observed in the strata oriens (Or) and radiatum (Rad) of CA1-3 and the molecular layer (Mol) of dentate gyrus (DG). b) After intra-hippocampal injection of octreotide (OCT), sst2A receptor-immunoreactive neurons are detected in the pyramidal cell layer (Py) of CA1-3 and granular layer (Gr) of DG. c) IRAP-immunoreactivity is located in the principal cell layers of the hippocampal formation. d) In the CA1 of control rats, double-labeling immunohistochemistry reveals that IRAP is predominantly localized in pyramidal cell bodies (Py), whereas sst2A receptor immunoreactivity is diffusely distributed in strata oriens (Or) and radiatum (Rad). Inset shows sst2A receptor immunoreactivity in the pyramidal cells layer. e-g) In OCT-injected rats, double-labeling immunohistochemistry reveals colocalization of internalized sst2A receptor and IRAP in pyramidal neurons of CA1. Note that all hippocampal sst2A receptor-immunoreactive neurons are IRAP-positive. Only a subpopulation of IRAP-immunoreactive neurons is sst2A receptor-positive. Similar stainings were found in three different OCT-injected rats (three sections per animal). Scale bars: a-c, 400 μm; d-g, 40 μm.

Figure 2. Kinetics of sst2A receptor internalization in primary hippocampal neurons. In control neurons, the sst2A receptor immunoreactivity is predominantly located at the surface of perikarya and proximal dendrites. Conversely, IRAP immunofluorescence is mainly confined to intracellular vesicles overlapping with *trans*-Golgi network marker TGN38. Little colocalization is thus observed between sst2A receptor and IRAP. Treatment with the sst2A receptor agonist octreotide for 5, 10 or 20 min results in a massive redistribution of sst2A receptor immunoreactivity from the cell surface into intracellular vesicles, where it is colocalized with IRAP (yellow pseudocolor signal on sst2A/IRAP merged images) and TGN38 (white pseudocolor

signal on sst2A/IRAP/TGN38 merged images). Thirty neurons/group were analyzed from 3 independent experiments. OCT, octreotide. Scale bars: 10 μm.

Figure 3. Internalized sst2A receptor colocalizes with IRAP in primary hippocampal neurons. The sst2A receptor immunoreactivity is confined to bright fluorescent granules in the cytoplasm of octreotide-treated neurons and colocalizes with IRAP-positive vesicles (arrows) as illustrated by high resolution confocal microscopy in three different neurons. Scale bars: 2 μm.

Figure 4. Kinetics of sst2A receptor recycling in primary hippocampal neurons. Fifteen minutes after agonist washout, only intracellular sst2A receptor immunoreactivity is apparent. Thirty min after OCT washout, the large majority of sst2A receptor immunofluorescence is still intracellular. However, membrane-associated receptors become apparent in perikarya and proximal dendrites. From 60 to 120 min after agonist washout, the surface sst2A receptor labeling becomes more and more intense. In parallel, the intensity of intracellular immunofluorescence gradually decreases. At 180 min after OCT washout, the distribution of sst2A receptor immunoreactivity is very similar to control conditions (i.e. before agonist-induced internalization of the receptor). The colocalization of sst2A receptor with IRAP (yellow pseudocolor signal on sst2A/IRAP merged images) and *trans*-Golgi network marker TGN38 (white pseudocolor signal on sst2A/IRAP/TGN38 merged images) is important at 30 min after octreotide washout and gradually decreases from 60 to 180 min. Thirty neurons/group were analyzed from 3 independent experiments. OCT, octreotide. Scale bars: 10 μm.

Figure 5. IRAP ligands accelerate sst2A receptor recycling in hippocampal neurons. At 45 min after OCT washout, sst2A receptor immunoreactivity is localized in the cytoplasm, overlapping with the *trans*-Golgi network marker TGN38, as well as at the cell surface in a form of a fluorescent ring (arrows). Note that the surface sst2A receptor labeling is more intense in

the Ang IV-treated neuron than in the PBS control. OCT, octreotide; PBS, phosphate-buffered saline. Scale bars: 10 μm.

Figure 6. Analysis of sst2A receptor recycling in hippocampal neurons. a) For semiquantitative analysis, a single optical section is acquired from the neuronal cell body at a z-axis level where the sst2A receptor labeling at the plasma membrane is identified as a line-like ring in the green channel around the TGN38 labeling of the red channel. Scale bar: 10 μm. b) Semiquantitative analysis reveals a significantly higher sst2A receptor immunofluorescence at the plasma membrane 30, 45 and 60 min after OCT washout in the Ang IV-treated neurons as compared to the respective PBS controls (upper panel). The sst2A receptor signal intensity is higher at the plasma membrane 45 min after OCT or SRIF washout in the Ang IV-treated group as compared to the respective PBS controls. Note, that no significant difference is detected between respective OCT- and SRIF-treated groups (lower panel). Thirty neurons/group were analyzed from 3 independent experiments. Values are expressed in relation to an arbitrary unit (100%) of the control value (PBS w/o agonist). ***$p < 0.001$; ns, not significant (ANOVA followed by Bonferroni's Multiple Comparison Test). Ang IV, angiotensin IV; OCT, octreotide; PBS, phosphate-buffered saline.

Figure 7. IRAP ligands do not bind to the sst2A receptor in stably transfected CHO-K1 cells. The specific binding of Ang IV (a) and LVV-H7 (b) to sst2A receptors in CHO-K1 cells was investigated by incubating these cells with increasing concentrations (10^{-9} M to 10^{-5} M) of IRAP ligands and 0.5 nM radiolabeled SRIF. In four independent experiments, the ^{125}I-labeled SRIF and IRAP ligands competed for binding to sst2A receptors, after which the number of counts per minute were measured. The results are shown as the percentage of ^{125}I-labeled SRIF binding to sst2A receptors. Ang IV, angiotensin IV; LVV-H7, LVV-Hemorphin 7.

Figure 8. IRAP-targeting shRNAs decreases IRAP immunoreactivity in hippocampal neurons. a) Using TurboGFP lentiviral particles with three IRAP-targeting shRNAs (IRAP LV-shRNA1-3) and a non-targeting control (NT LV-shRNA), neuronal transduction is demonstrated by the presence of the TurboGFP signal (green). In neurons transduced with non-targeting LV-shRNA, IRAP immunoreactivity is mainly confined to vesicles in the cell bodies and proximal dendrites (red). Note that in neurons transduced with IRAP-targeting shRNA, the intensity of IRAP immunofluorescence is low. Scale bars: 10 μm. b) Semiquantitative analysis reveals that the intensity of IRAP immunoreactivity in the IRAP LV-shRNA1-3 groups is significantly lower as compared to the NT LV-shRNA controls. Thirty neurons/group were analyzed from 3 independent experiments. ***$p < 0.001$ (ANOVA followed by Bonferroni's Multiple Comparison Test).

Figure 9. IRAP knockdown increases sst2A receptor recycling in hippocampal neurons. a) Using TurboGFP lentiviral particles with three IRAP-targeting shRNAs (IRAP LV-shRNA1-3) and a non-targeting control (NT LV-shRNA), neuronal transduction is demonstrated by the presence of the TurboGFP signal. At 45 min after agonist washout, in neurons transduced with both non-targeting and IRAP-targeting shRNA, the sst2A receptor immunoreactivity is localized in the cytoplasm, overlapping with the *trans*-Golgi marker TGN38. Receptors are also localized at the cell surface (arrows). Note, however, that the intensity of the surface sst2A receptor labeling is higher in neurons transduced with IRAP LV-shRNAs than those with the NT LV-shRNA control. Scale bars: 10 μm. b) Semiquantitative analysis reveals that the intensity of sst2A receptor immunoreactivity at the plasma membrane 45 min after OCT washout is significantly higher in the IRAP LV-shRNA1-3 groups as compared to the NT LV-shRNA control. Thirty neurons/group were analyzed from 3 independent experiments. Values are expressed in relation to an arbitrary unit (100%) of the control value (NT LV-shRNA). ***$p < 0.001$ (ANOVA followed by Bonferroni's Multiple Comparison Test). OCT, octreotide.

Figure 10. IRAP ligands display anticonvulsive properties in the rat focal pilocarpine model. Time profiles of seizure severity scores (SSS) are shown with total seizure severity score (TSSS) in the inserts. Both Ang IV (a) and LVV-H7 (b) treatments at 10 μM concentration result in a significantly lower SSS and TSSS. **p < 0.01; ***p < 0.001 vs. pilocarpine control group (SSS: two-way ANOVA followed by Dunnett's Multiple Comparison Test; TSSS: ANOVA followed by Bonferroni's Multiple Comparison Test). Ang IV, angiotensin IV; LVV-H7, LVV-Hemorphin 7.

Figure 11. Antagonists of the sst2A receptor prevent the anticonvulsive effect of Ang IV and LVV-H7 in the rat focal pilocarpine model. The sst2A receptor antagonist cyanamid 154806 (a and c) or BIM-23627 (b) reverse the effect of Ang IV (a, b) and LVV-H7 (c) on total seizure severity score (TSSS). *p < 0.05; **p < 0.01 between groups (ANOVA followed by Bonferroni's Multiple Comparison Test). Ang IV, angiotensin IV; LVV-H7, LVV-Hemorphin 7.

Figure 12. Angiotensin AT1 (a) and μ/κ (b) receptors are not implicated in the anticonvulsive effect of Ang IV and LVV-H7 in the focal pilocarpine model. AT1 receptor antagonist Candesartan (a) and the opioid μ/k receptor antagonist Naltrexone (b) have no significant effect on seizure severity as compared to the pilocarpine control group. Furthermore, pre-treatment with Candesartan or Naltrexone does not abolish the anticonvulsive effect of Ang IV. **p < 0.01; ns, not significant compared to the pilocarpine control group (ANOVA followed by Bonferroni's Multiple Comparison Test). TSSS, total seizure severity score; Ang IV, angiotensin IV; LVV-H7, LVV-Hemorphin 7.

Figure 13. Administration of Ang IV and LVV-H7 does not decrease hippocampal SRIF concentration. Administration of Ang IV or LVV-H7 has no effect on SRIF concentration of

hippocampal microdialysates (two-way ANOVA followed by Bonferroni's Multiple Comparison Test: Ang IV or LVV-H7 vs. aCSF control group). aCSF, artificial cerebrospinal fluid; Ang IV, angiotensin IV; LVV-H7, LVV-Hemorphin 7.

Figure 14. Ang IV potentiates the anticonvulsive effect of SRIF in the focal pilocarpine model. A combination of subthreshold concentrations (i.e. ineffective on pilocarpine-induced seizures) of Ang IV (1 µM) and SRIF (0.1 µM) significantly reduces behavioral seizures (a) compared to the pilocarpine control group. In rats treated with both Ang IV and SRIF, EEG seizure duration is not significantly different (b), while the latency to first EEG seizure is significantly higher (c) compared to the pilocarpine control group. The TSSS is positively correlated with EEG seizure duration (c) and negatively correlated with EEG seizure latency (d). Representative EEG traces are shown in (f) with (g) illustrating baseline EEG activity (left panels) and typical spike-wave activity 40 min following the onset of pilocarpine administration (right panels). *$p < 0.05$; **$p < 0.01$ compared to the pilocarpine control group (ANOVA followed by Bonferroni's Multiple Comparison Test). TSSS, total seizure severity score; Ang IV, angiotensin IV; LVV-H7, LVV-Hemorphin 7.

Figure 15. Ang IV increases *in vivo* the density of sst2A receptors at the plasma membrane in pilocarpine-treated rats. a,b) In pilocarpine control rats, many sst2A receptor immunoparticles are intracellular (arrows) in dendrites (a) and dendritic spines (inset of a) of CA1 pyramidal neurons. In the pilocarpine group which received intra-hippocampal perfusion of Ang IV, numerous sst2A receptor immunoparticles are located at the plasma membrane (arrowheads) of dendrites (b) and dendritic spines (inset of b) of CA1 pyramidal neurons. Scale bar: 500 nm. c) In pilocarpine control rats, the largest proportion of sst2A receptor immunoparticles are intracellular in CA1 pyramidal cell dendrites, only 28.6% of them are associated with the plasma membrane. By contrast, in the pilocarpine group treated with Ang IV,

70.5% of sst2A receptor immunoparticles are at the plasma membrane of CA1 pyramidal cell dendrites. d) Statistical analysis reveals that the density of immunoparticles is significantly higher at the plasma membrane and lower intracellularly in the Ang IV-treated pilocarpine group as compared to the pilocarpine controls. Note that the total number of immunoparticles is not different between the two groups. Ten dendrites/animal were analyzed in 3 control and Ang IV-treated rats. Values are expressed in relation to an arbitrary unit (100%) of the control values. **p < 0.01; ***p < 0.001; ns, not significant (Mann-Whitney U test). Ang IV, angiotensin IV; IC, intracellular; PM, plasma membrane.

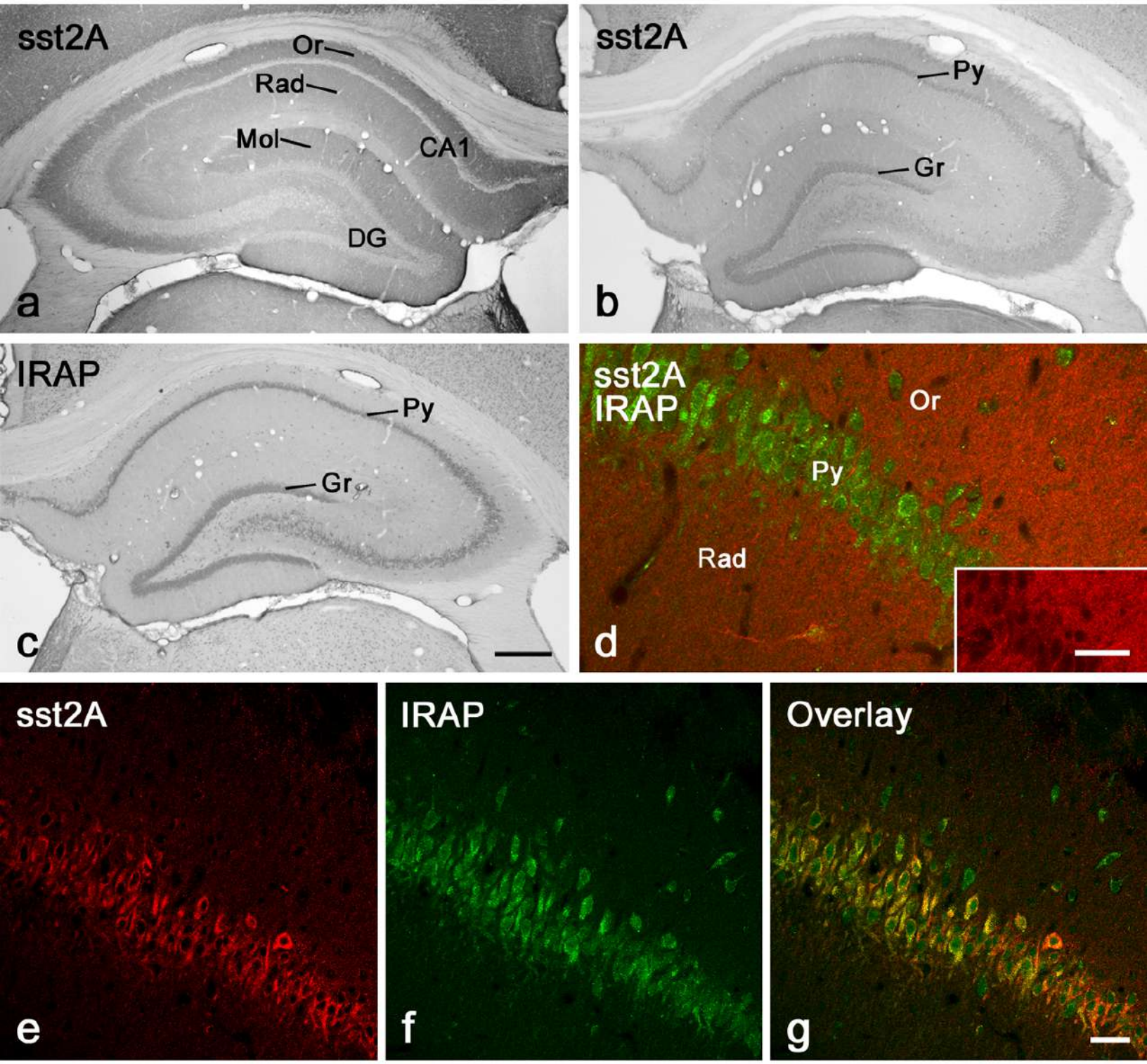
sst2A
Or
Rad
Mol
CA1
DG
a
sst2A
Py
Gr
b
IRAP
Py
Gr
c
sst2A
IRAP
Or
Py
Rad
d
sst2A
e
IRAP
f
Overlay
g

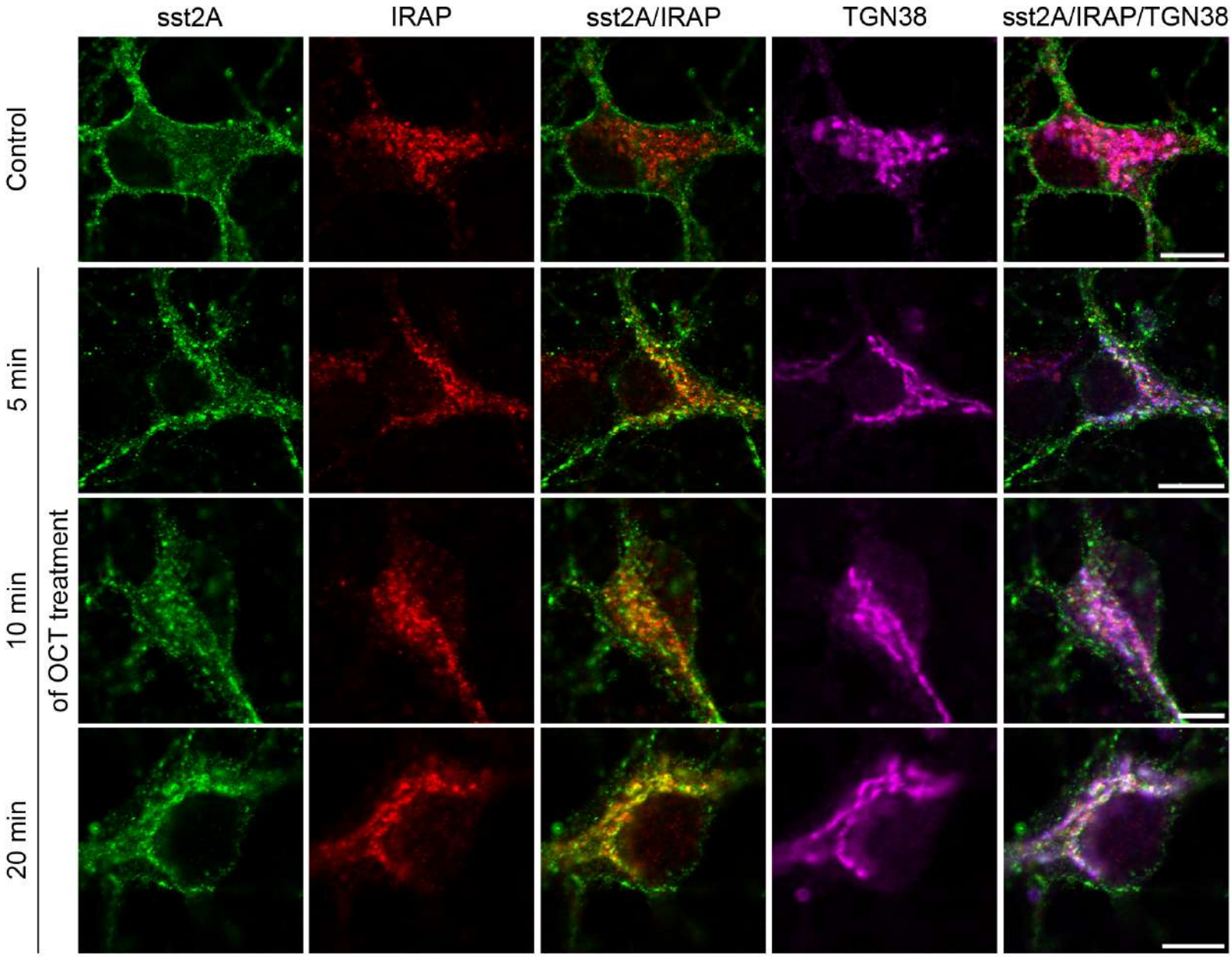
sst2A
IRAP
sst2A/IRAP
TGN38
sst2A/IRAP/TGN38
Control
5 min
10 min
20 min
of OCT treatment

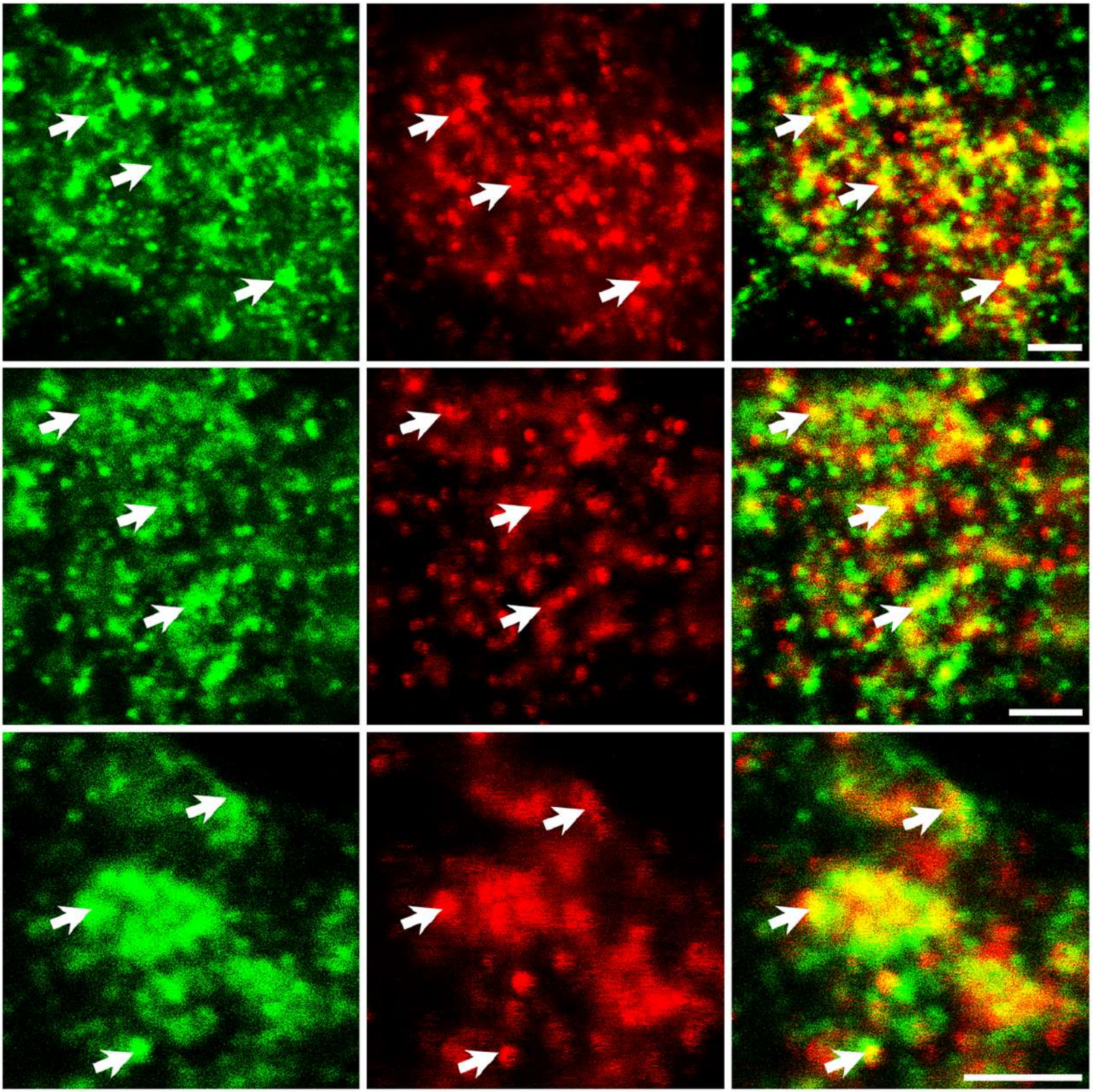
sst2A
IRAP
sst2A/IRAP

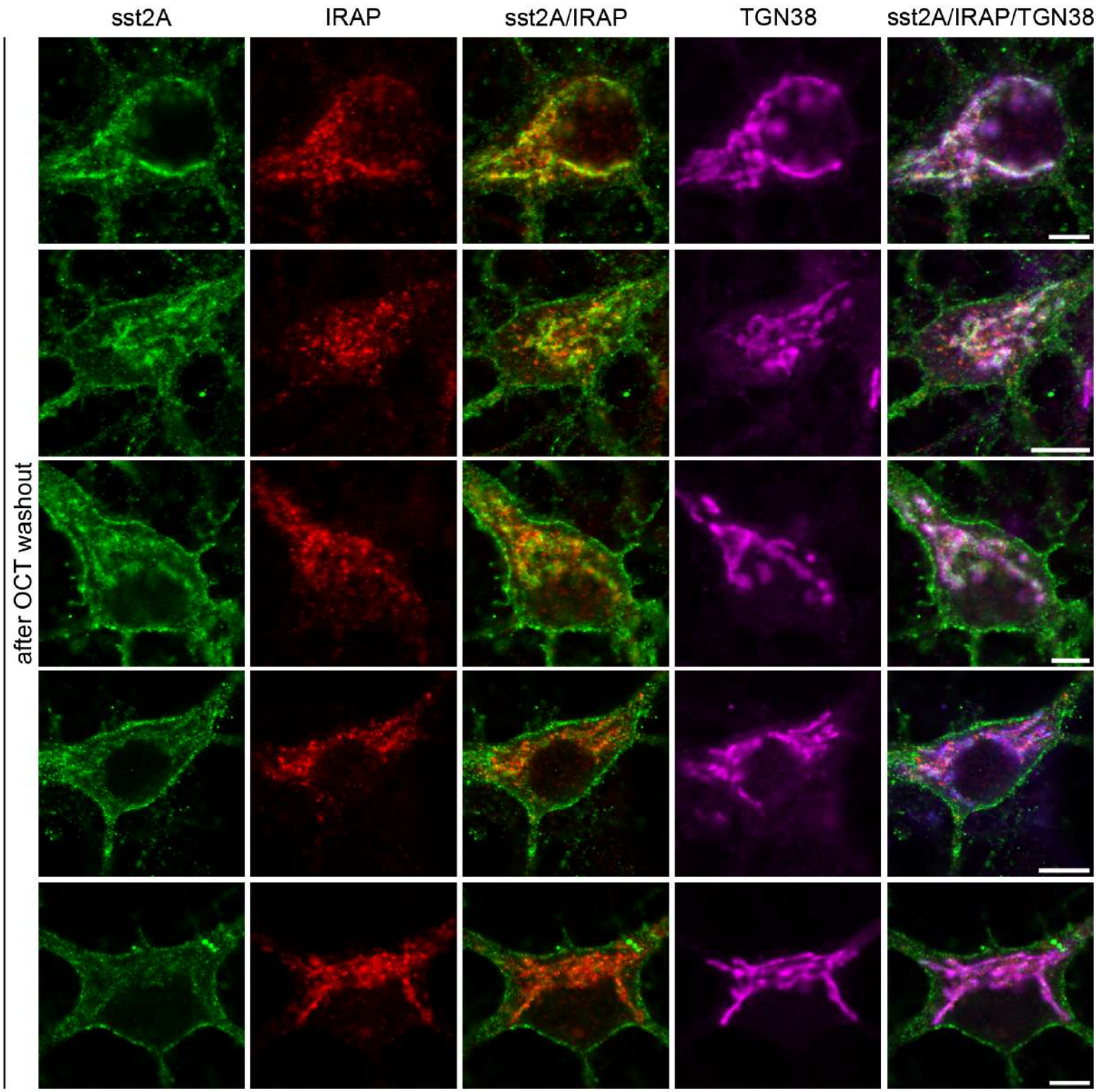
sst2A
IRAP
sst2A/IRAP
TGN38
sst2A/IRAP/TGN38
15 min
30 min
60 min
120 min
180 min
after OCT washout

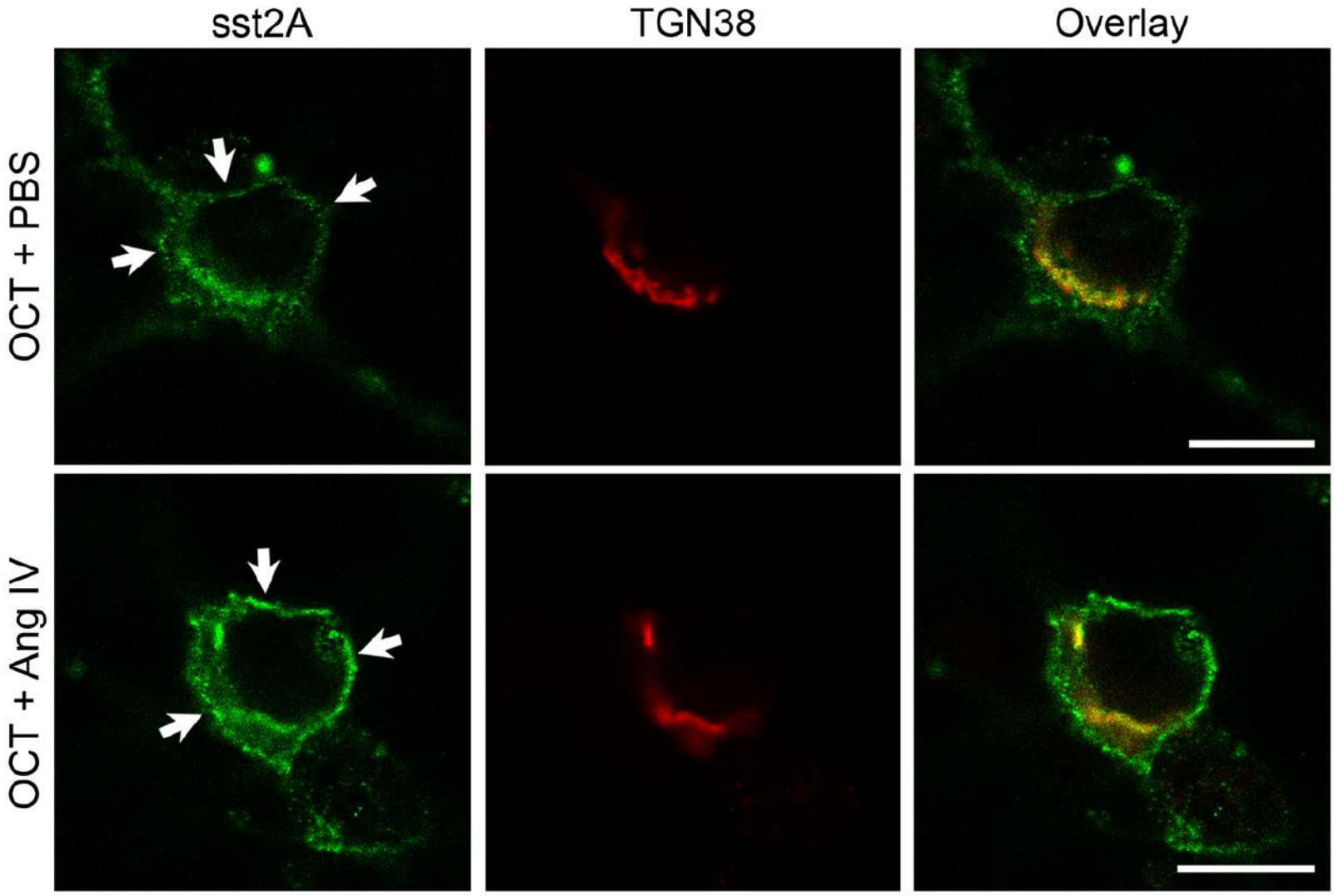
sst2A
TGN38
Overlay
OCT + PBS
OCT + Ang IV

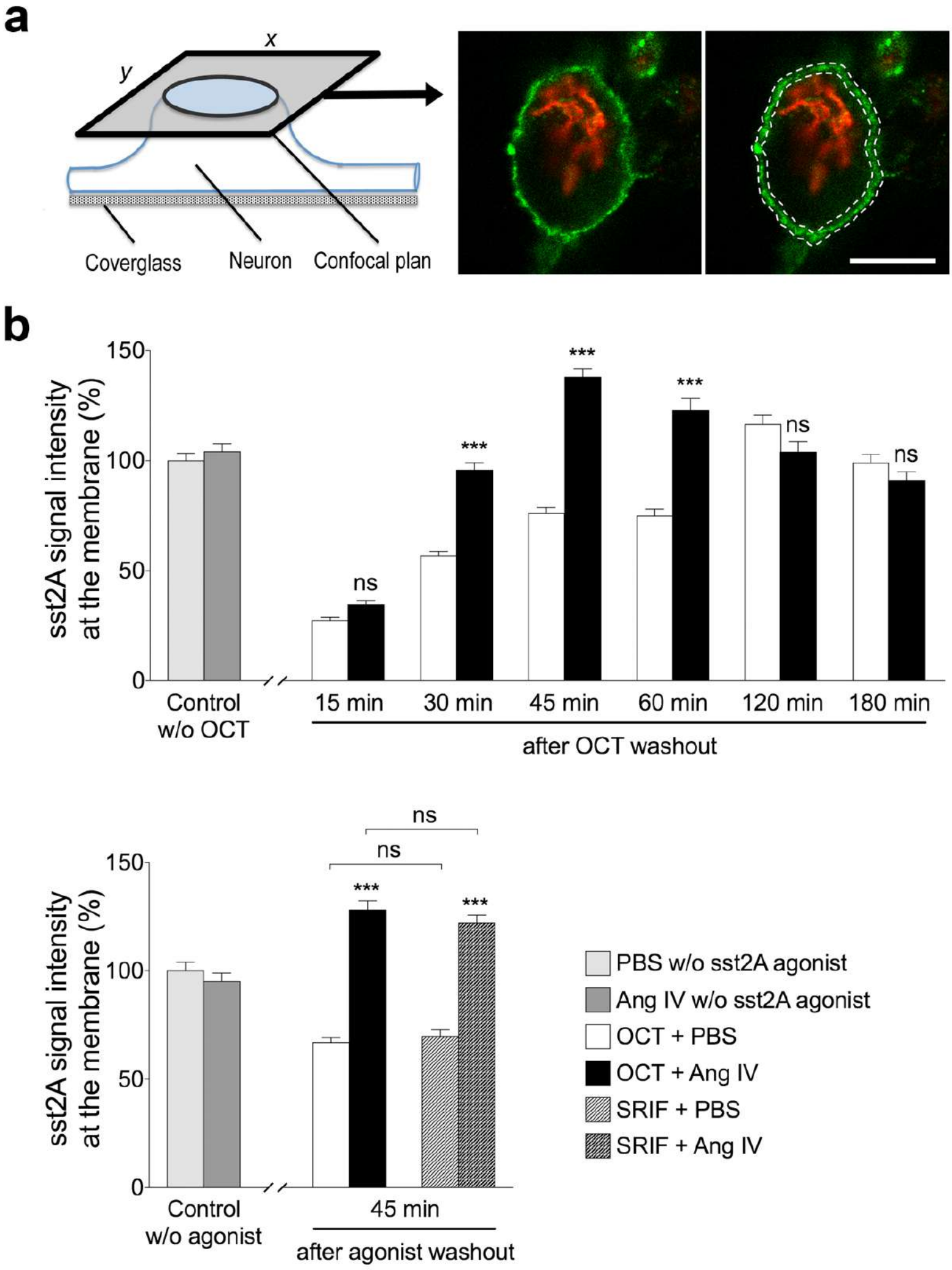
a
x
y
Coverglass
Neuron
Confocal plan
b
sst2A signal intensity at the membrane (%)
150
100
50
0
***
***
***
ns
ns
ns
Control w/o OCT
15 min
30 min
45 min
60 min
120 min
180 min
after OCT washout
ns
ns
***
***
Control w/o agonist
45 min
after agonist washout
PBS w/o sst2A agonist
Ang IV w/o sst2A agonist
OCT + PBS
OCT + Ang IV
SRIF + PBS
SRIF + Ang IV

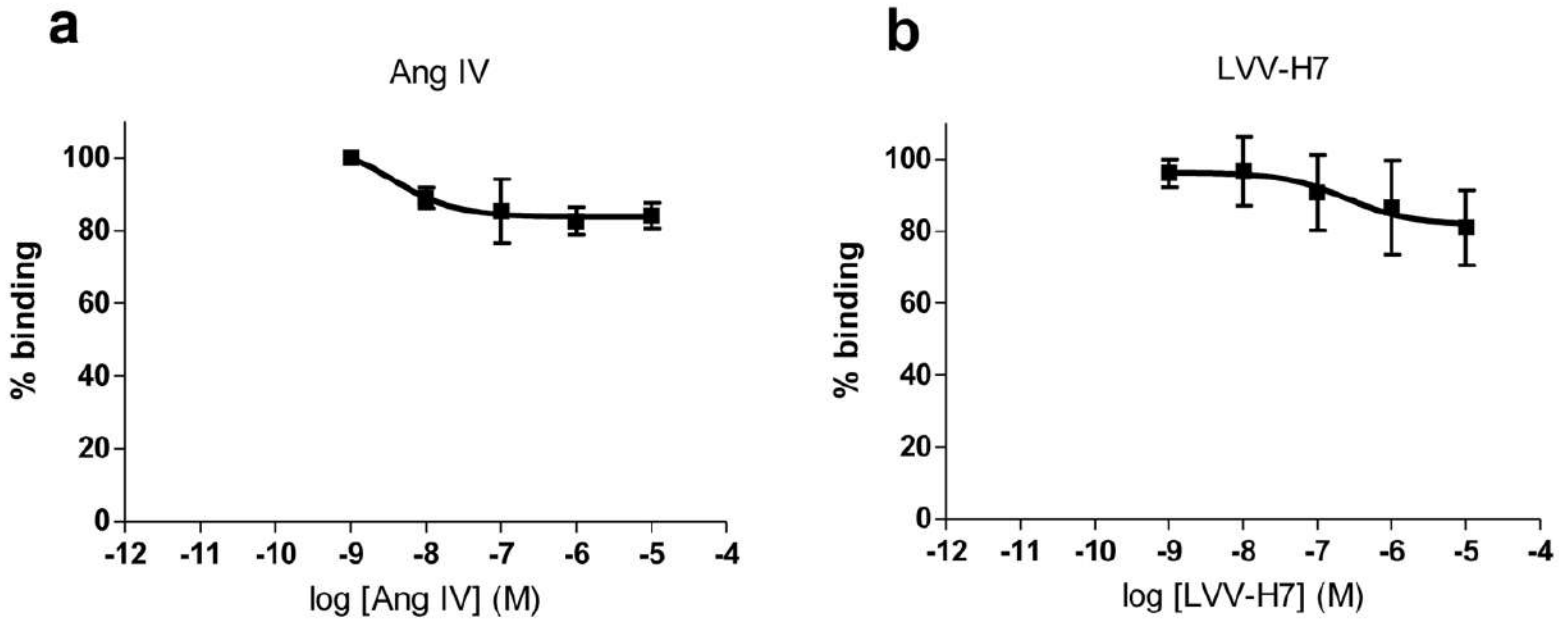
a
Ang IV
% binding
100
80
60
40
20
0
-12
-11
-10
-9
-8
-7
-6
-5
-4
log [Ang IV] (M)
b
LVV-H7
% binding
100
80
60
40
20
0
-12
-11
-10
-9
-8
-7
-6
-5
-4
log [LVV-H7] (M)

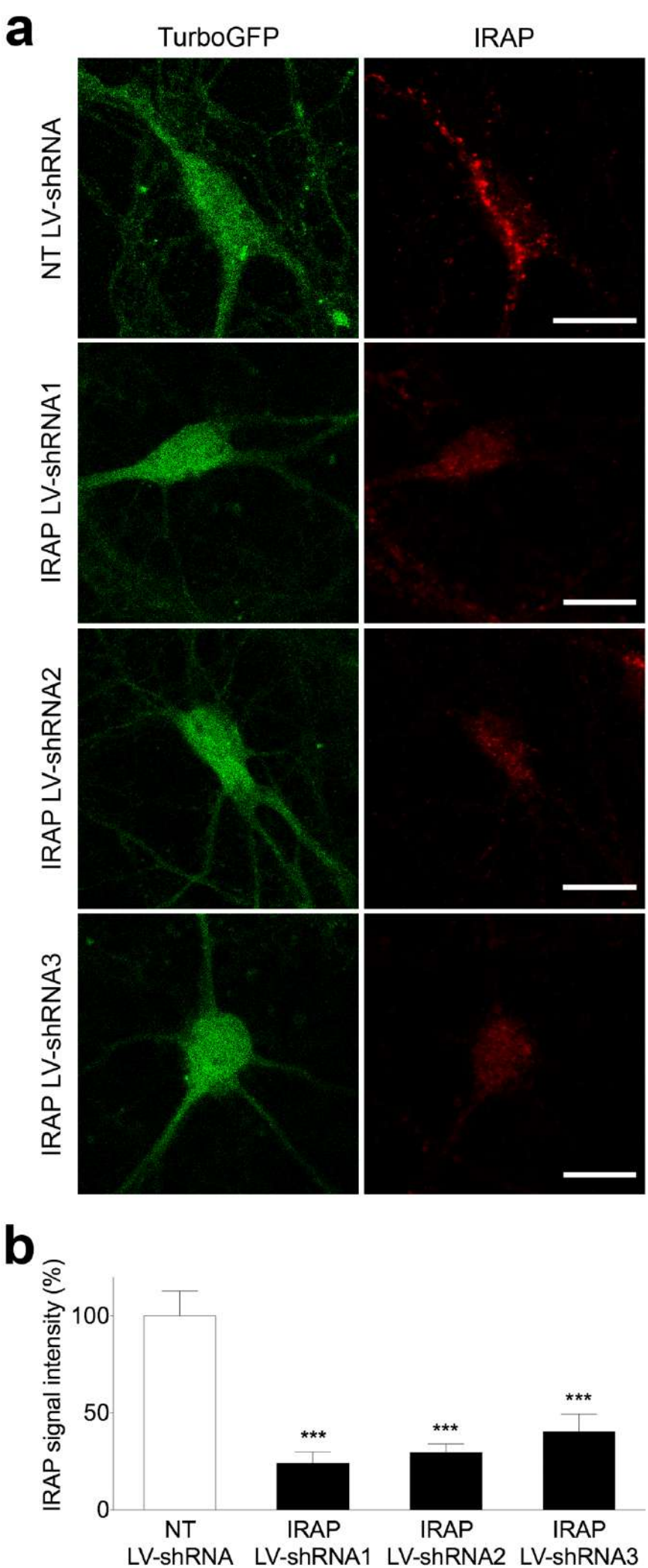
a
TurboGFP
IRAP
NT LV-shRNA
IRAP LV-shRNA1
IRAP LV-shRNA2
IRAP LV-shRNA3
b
IRAP signal intensity (%)
100
50
0
***
***
***
NT LV-shRNA
IRAP LV-shRNA1
IRAP LV-shRNA2
IRAP LV-shRNA3

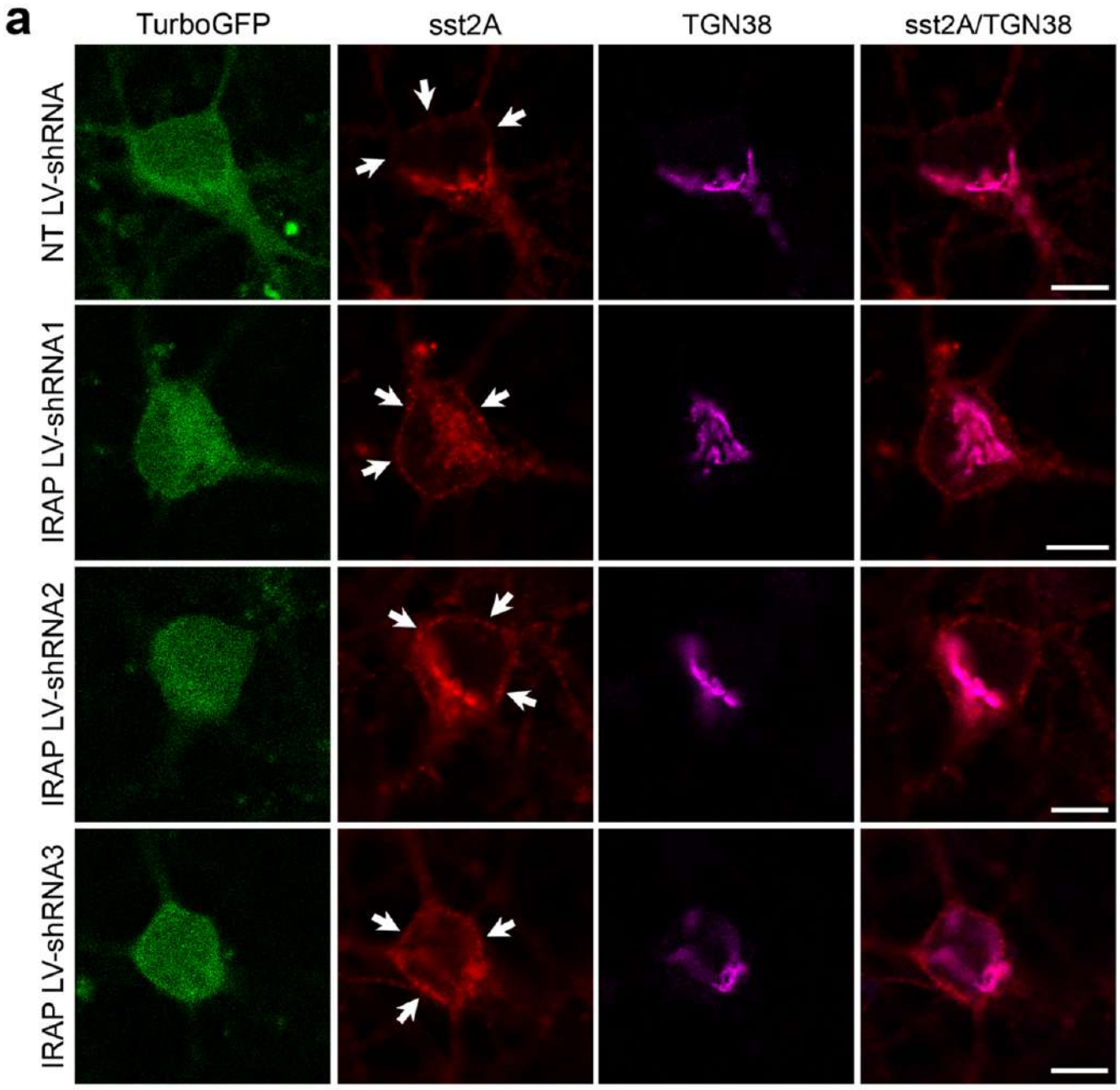
a
TurboGFP
sst2A
TGN38
sst2A/TGN38
NT LV-shRNA
IRAP LV-shRNA1
IRAP LV-shRNA2
IRAP LV-shRNA3

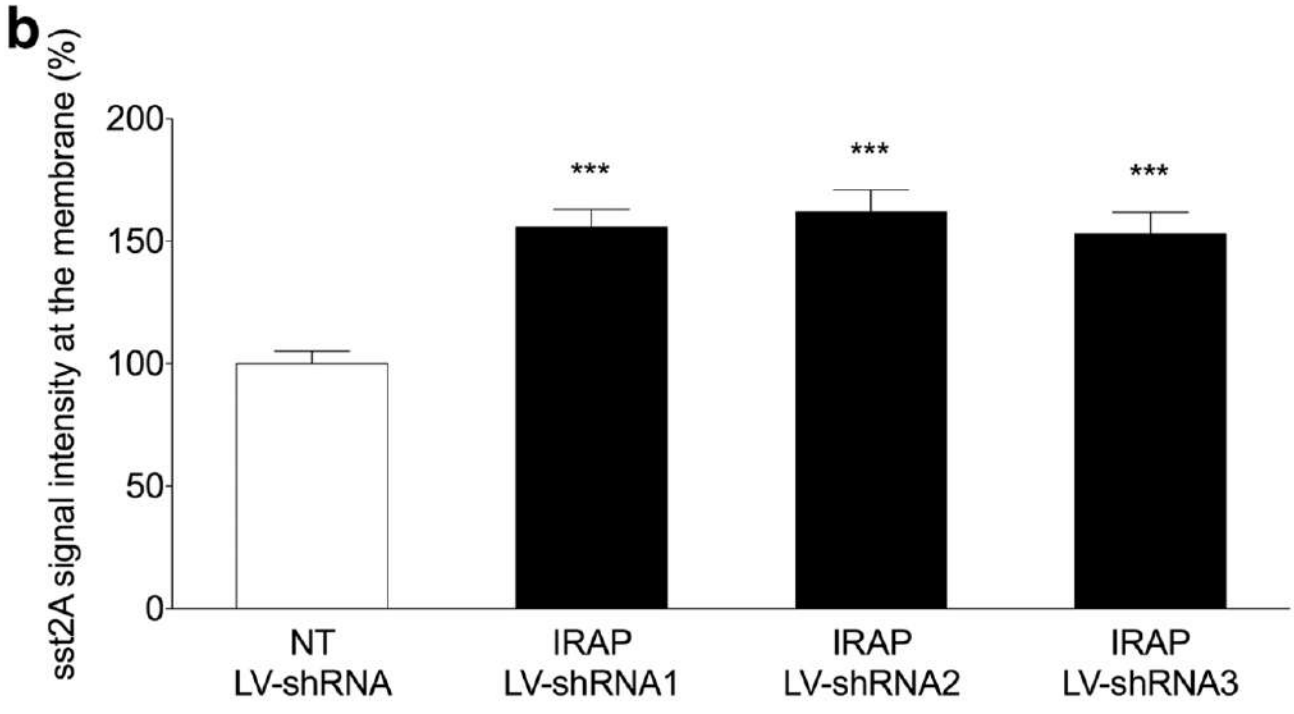
b
sst2A signal intensity at the membrane (%)
200
150
100
50
0
***
***
***
NT
LV-shRNA
IRAP
LV-shRNA1
IRAP
LV-shRNA2
IRAP
LV-shRNA3

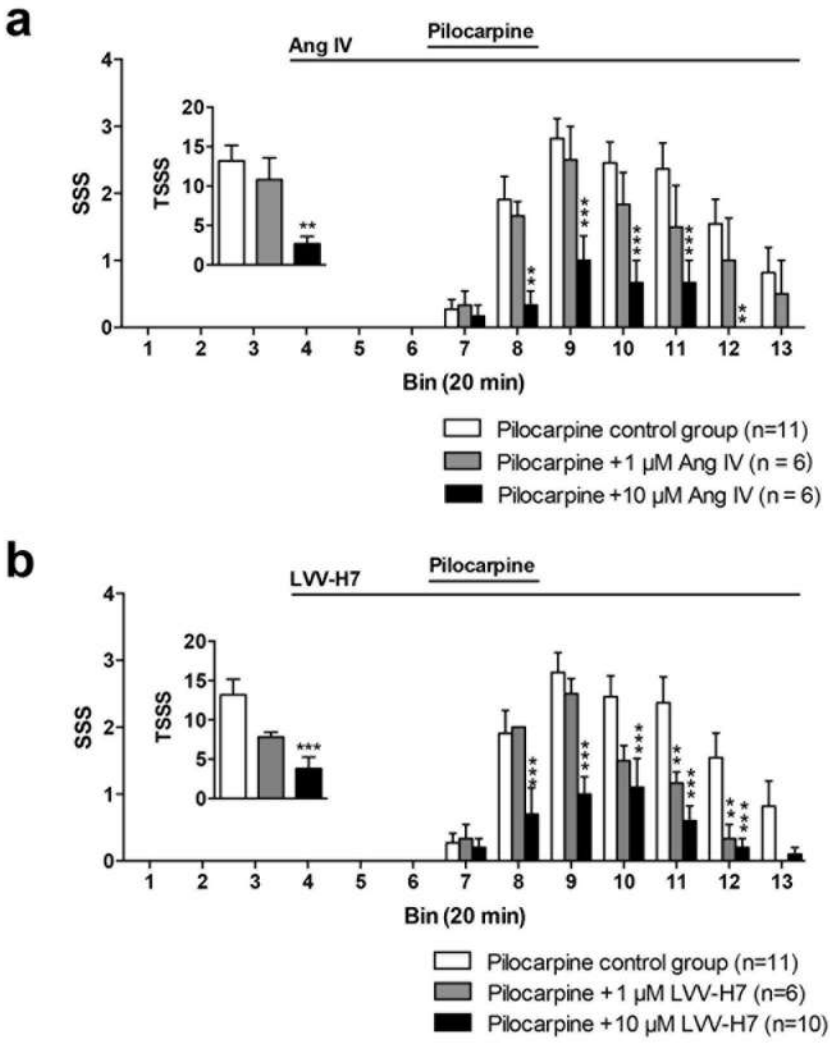
a
Ang IV
Pilocarpine
SSS
TSSS
Bin (20 min)
Pilocarpine control group (n=11)
Pilocarpine +1 μM Ang IV (n = 6)
Pilocarpine +10 μM Ang IV (n = 6)
b
LVV-H7
Pilocarpine
SSS
TSSS
Bin (20 min)
Pilocarpine control group (n=11)
Pilocarpine +1 μM LVV-H7 (n=6)
Pilocarpine +10 μM LVV-H7 (n=10)

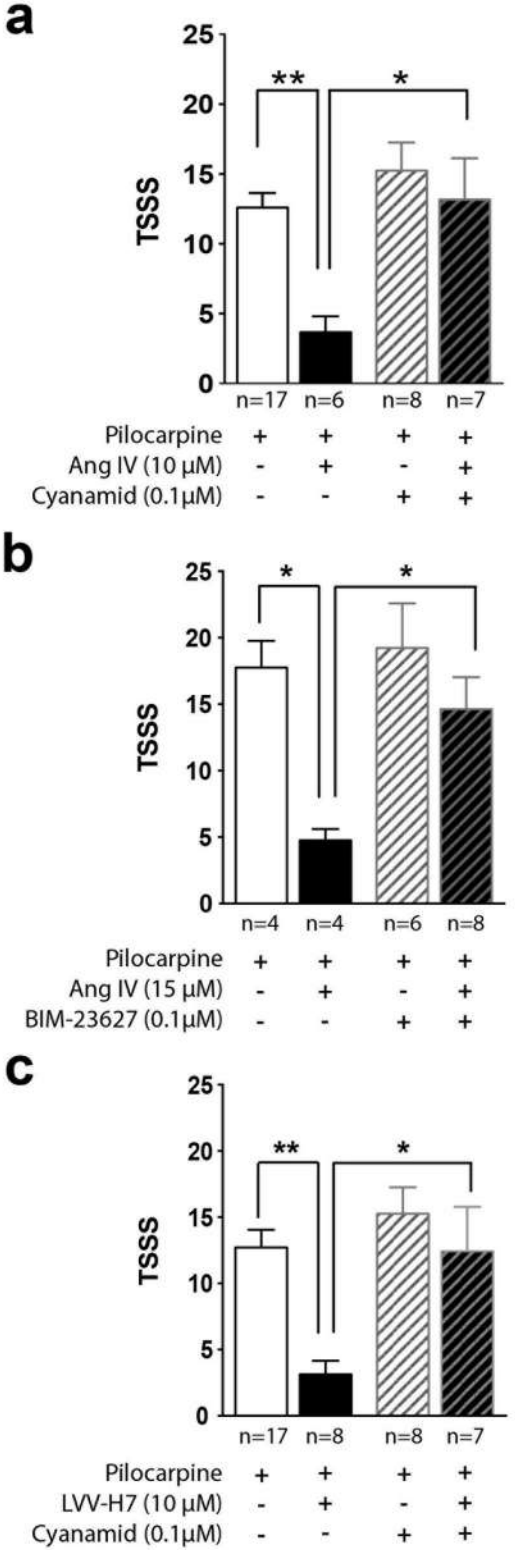
a
TSSS
25
20
15
10
5
0
**
*
n=17 n=6 n=8 n=7
Pilocarpine + + + +
Ang IV (10 μM) - + - +
Cyanamid (0.1μM) - - + +
b
TSSS
25
20
15
10
5
0
*
*
n=4 n=4 n=6 n=8
Pilocarpine + + + +
Ang IV (15 μM) - + - +
BIM-23627 (0.1μM) - - + +
c
TSSS
25
20
15
10
5
0
**
*
n=17 n=8 n=8 n=7
Pilocarpine + + + +
LVV-H7 (10 μM) - + - +
Cyanamid (0.1μM) - - + +

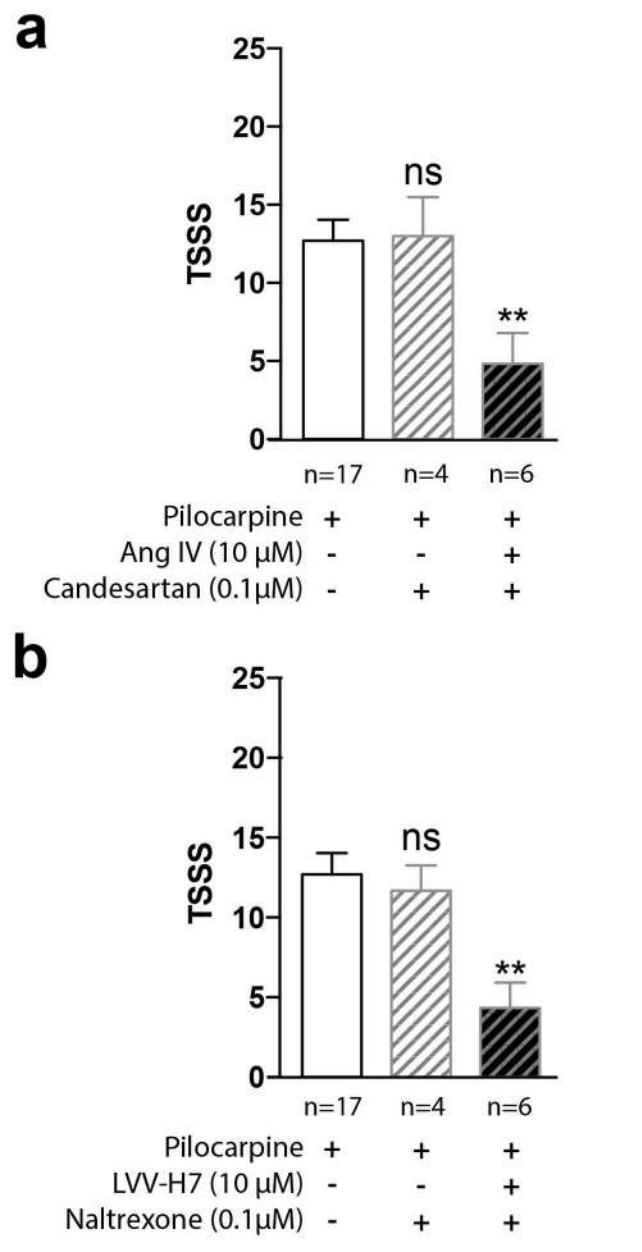
a
25
20
15
10
5
0
TSSS
ns
**
n=17
n=4
n=6
Pilocarpine + + +
Ang IV (10 μM) - - +
Candesartan (0.1μM) - + +
b
25
20
15
10
5
0
TSSS
ns
**
n=17
n=4
n=6
Pilocarpine + + +
LVV-H7 (10 μM) - - +
Naltrexone (0.1μM) - + +

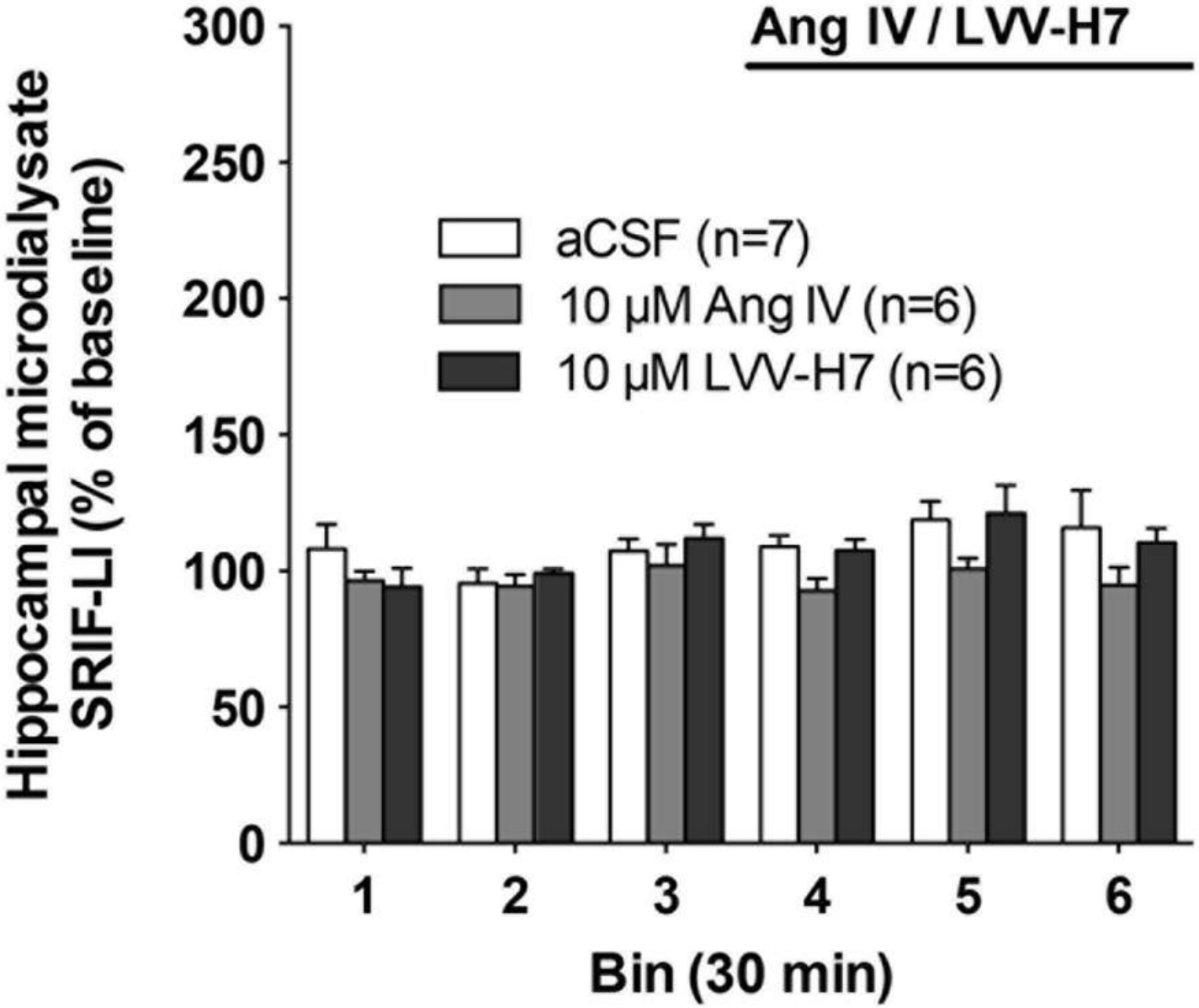
Ang IV / LVV-H7
aCSF (n=7)
10 μM Ang IV (n=6)
10 μM LVV-H7 (n=6)
Hippocampal microdialysate
SRIF-LI (% of baseline)
300
250
200
150
100
50
0
1
2
3
4
5
6
Bin (30 min)

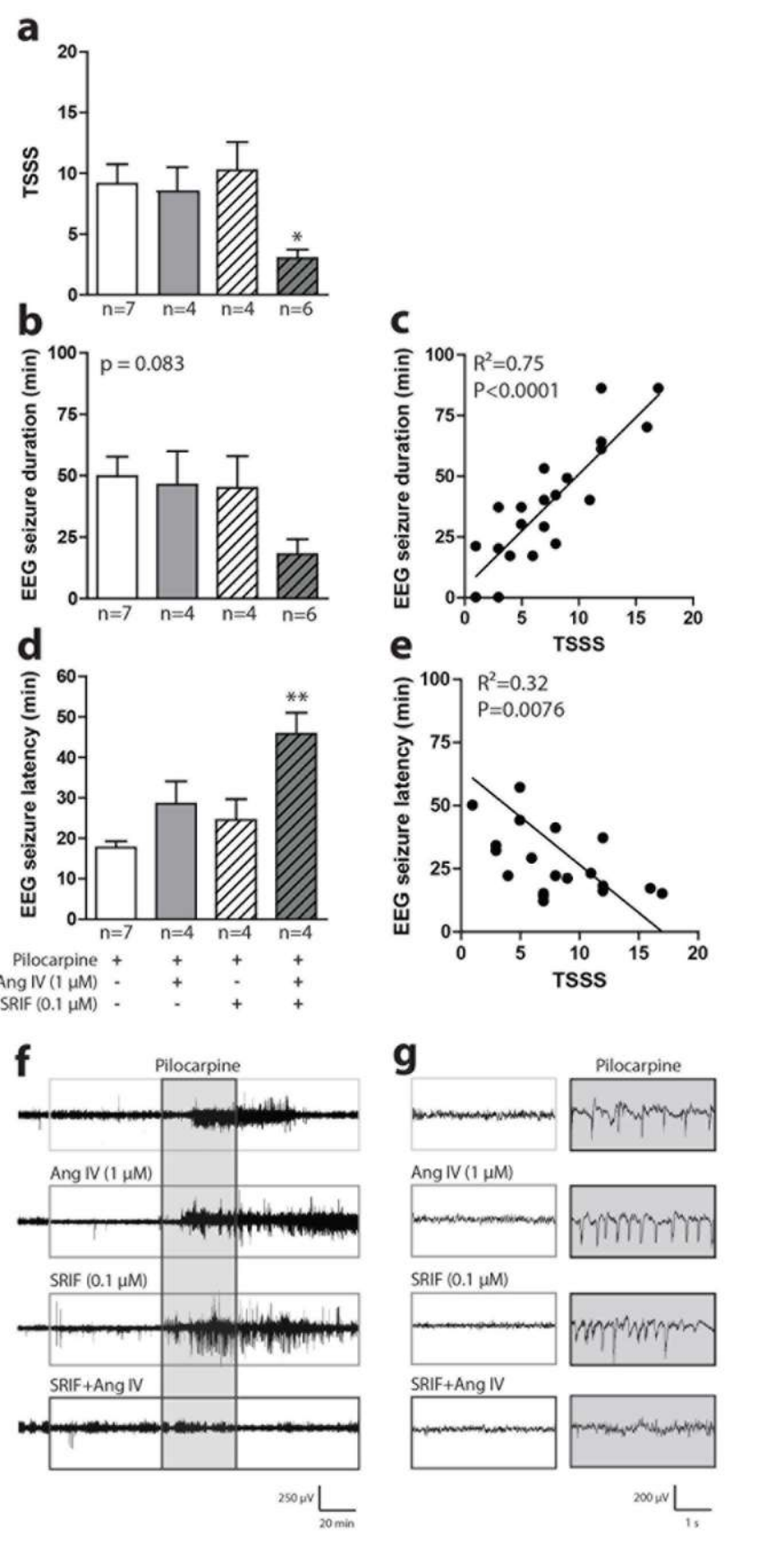
a
TSSS
20
15
10
5
0
*
n=7
n=4
n=4
n=6
b
EEG seizure duration (min)
p = 0.083
100
75
50
25
0
n=7
n=4
n=4
n=6
c
EEG seizure duration (min)
R²=0.75
P<0.0001
100
75
50
25
0
0
5
10
15
20
TSSS
d
EEG seizure latency (min)
60
50
40
30
20
10
0
**
n=7
n=4
n=4
n=4
Pilocarpine + + + +
Ang IV (1 µM) - + - +
SRIF (0.1 µM) - - + +
e
EEG seizure latency (min)
R²=0.32
P=0.0076
100
75
50
25
0
0
5
10
15
20
TSSS
f
Pilocarpine
Ang IV (1 µM)
SRIF (0.1 µM)
SRIF+Ang IV
250 µV
20 min
g
Pilocarpine
Ang IV (1 µM)
SRIF (0.1 µM)
SRIF+Ang IV
200 µV
1 s

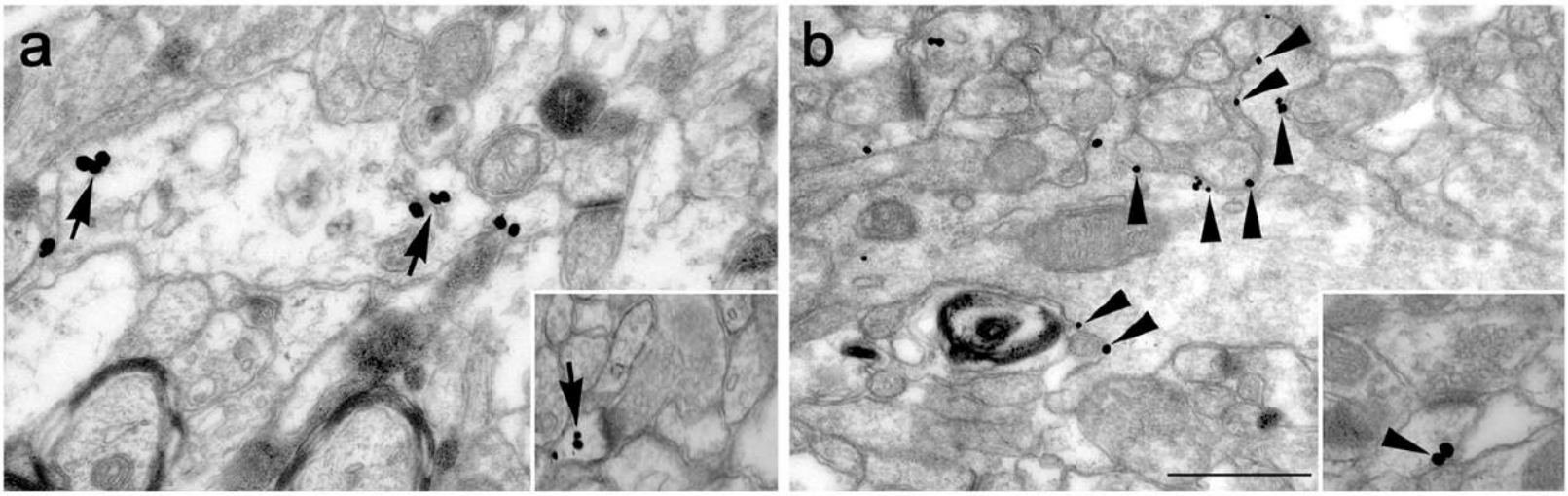
a
b

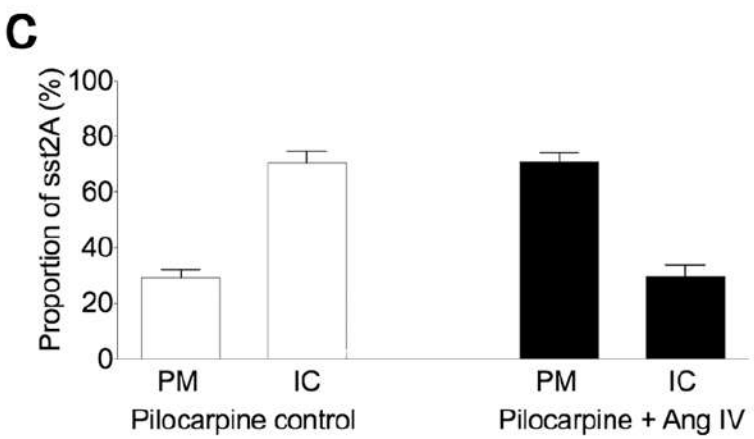
c
Proportion of sst2A (%)
100
80
60
40
20
0
PM
IC
PM
IC
Pilocarpine control
Pilocarpine + Ang IV

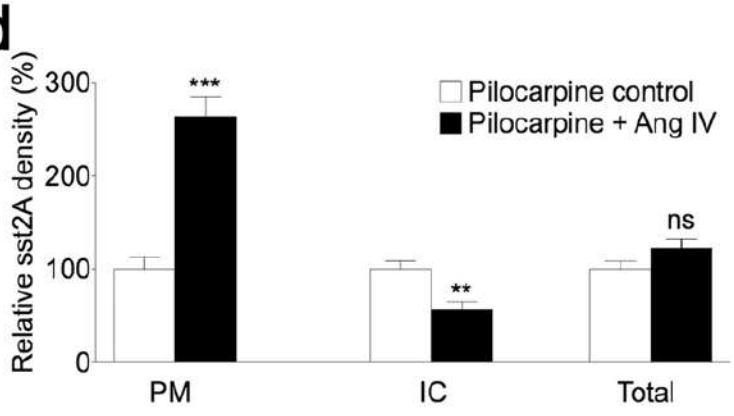
d
Relative sst2A density (%)
300
200
100
0
***
**
ns
Pilocarpine control
Pilocarpine + Ang IV
PM
IC
Total